



**Calhoun: The NPS Institutional Archive**  
**DSpace Repository**

---

Theses and Dissertations

1. Thesis and Dissertation Collection, all items

---

2001-03

## Vortex ripple morphology using Dune2D model

Martin, Stephen D.

Monterey, California. Naval Postgraduate School

---

<https://hdl.handle.net/10945/2268>

---

This publication is a work of the U.S. Government as defined in Title 17, United States Code, Section 101. Copyright protection is not available for this work in the United States.

*Downloaded from NPS Archive: Calhoun*



<http://www.nps.edu/library>

Calhoun is the Naval Postgraduate School's public access digital repository for research materials and institutional publications created by the NPS community. Calhoun is named for Professor of Mathematics Guy K. Calhoun, NPS's first appointed -- and published -- scholarly author.

**Dudley Knox Library / Naval Postgraduate School**  
**411 Dyer Road / 1 University Circle**  
**Monterey, California USA 93943**

# NAVAL POSTGRADUATE SCHOOL

## Monterey, California



## THESIS

**VORTEX RIPPLE MORPHOLOGY USING DUNE2D MODEL**

by

Stephen D. Martin

March 2001

Thesis Advisor:  
Thesis Co-Advisor:

Edward B. Thornton  
Timothy P. Stanton

Approved for public release; distribution is unlimited

20010531 056

<b>REPORT DOCUMENTATION PAGE</b>			Form Approved OMB No. 0704-0188	
Public reporting burden for this collection of information is estimated to average 1 hour per response, including the time for reviewing instruction, searching existing data sources, gathering and maintaining the data needed, and completing and reviewing the collection of information. Send comments regarding this burden estimate or any other aspect of this collection of information, including suggestions for reducing this burden, to Washington headquarters Services, Directorate for Information Operations and Reports, 1215 Jefferson Davis Highway, Suite 1204, Arlington, VA 22202-4302, and to the Office of Management and Budget, Paperwork Reduction Project (0704-0188) Washington DC 20503.				
<b>1. AGENCY USE ONLY (Leave blank)</b>		<b>2. REPORT DATE</b> Mar 2001	<b>3. REPORT TYPE AND DATES COVERED</b> Master's Thesis	
<b>4. TITLE AND SUBTITLE:</b> Vortex Ripple Morphology using DUNE2D Model			<b>5. FUNDING NUMBERS</b>	
<b>6. AUTHOR(S)</b> Martin, Stephen D.				
<b>7. PERFORMING ORGANIZATION NAME(S) AND ADDRESS(ES)</b> Naval Postgraduate School Monterey, CA 93943-5000			<b>8. PERFORMING ORGANIZATION REPORT NUMBER</b>	
<b>9. SPONSORING / MONITORING AGENCY NAME(S) AND ADDRESS(ES)</b> Office of Naval Research			<b>10. SPONSORING / MONITORING AGENCY REPORT NUMBER</b>	
<b>11. SUPPLEMENTARY NOTES</b> The views expressed in this thesis are those of the author and do not reflect the official policy or position of the Department of Defense or the U.S. Government.				
<b>12a. DISTRIBUTION / AVAILABILITY STATEMENT</b> Approved for public release; distribution is unlimited (mix case letters)			<b>12b. DISTRIBUTION CODE</b>	
<b>13. ABSTRACT (maximum 200 words)</b>  The DUNE2D boundary layer model for small-scale morphology (Andersen, 1999) is compared with bedform morphology measured on the inner shelf in 11m water depth during the SHOWEX experiment at Duck, N.C. The model consists of inter-linked modules for flow, sediment transport and morphology. The flow module is based on solving the Reynold's averaged Navier-Stokes equations in the vertical plane with k-omega turbulence closure. The model has been extended to accept a general (but periodic) bottom boundary to be able to compare with field data. Boundary layer velocity profiles were measured using a Bistatic Coherent Doppler Velocity profiler (BCDV). A two-axis scanning sonar altimeter measured small-scale morphology over a 1 by 1.5 m area with 4 cm horizontal and 0.25 cm vertical resolutions. Bottom maps of small-scale morphology were obtained continuously every 20 minutes. A relatively simple data sequence was selected for model comparison, during which time the wave forcing evolved abruptly from $H_{sig}=0.3m$ to $H_{sig}=3.0m$ (bed velocity < 1 m/s), and the bed evolved from no motion (relic) to actively migrating vortex ripples. SHOWEX bedform changes under low wave plus collinear current conditions resulted in minor changes of the vortex ripple fields. Bedform migration rates of the model were similar to the field migration rates. Like the field data, the modeled data under strong forcing removed smaller scale vortex ripples and redistributed the sediment into a larger scale ripple with a large portion of sediments in suspension above the bed. Limitations of the model owing to the 2-D assumption, periodic boundaries and monochromatic wave forcing constraints are discussed.				
<b>14. SUBJECT TERMS</b> Waves, Bottom boundary layer, Nearshore dynamics, Sediment transport, Morphology.			<b>15. NUMBER OF PAGES</b> 84	
			<b>16. PRICE CODE</b>	
<b>17. SECURITY CLASSIFICATION OF REPORT</b> Unclassified	<b>18. SECURITY CLASSIFICATION OF THIS PAGE</b> Unclassified	<b>19. SECURITY CLASSIFICATION OF ABSTRACT</b> Unclassified	<b>20. LIMITATION OF ABSTRACT</b> UL	

THIS PAGE INTENTIONALLY LEFT BLANK

Approved for public release; distribution is unlimited

**VORTEX RIPPLE MORPHOLOGY USING DUNE2D MODEL**

Stephen D. Martin  
Lieutenant Commander, United States Navy  
B.S., United States Naval Academy, 1991  
M.S., The Pennsylvania State University, 1993

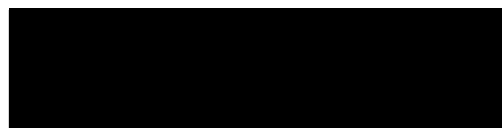
Submitted in partial fulfillment of the  
requirements for the degree of

**MASTER OF SCIENCE IN METEOROLOGY AND OCEANOGRAPHY**

from the

**NAVAL POSTGRADUATE SCHOOL**  
**March 2001**

Author:



Stephen D. Martin

Approved by:



Edward B. Thornton, Thesis Advisor



Timothy P. Stanton, Thesis Co-Advisor



Roland W. Garwood Jr., Chairman  
Oceanography Department

THIS PAGE INTENTIONALLY LEFT BLANK

## ABSTRACT

The DUNE2D boundary layer model for small-scale morphology (Andersen, 1999) is compared with bedform morphology measured on the inner shelf in 11m water depth during the SHOWEX experiment at Duck, N.C. The model consists of inter-linked modules for flow, sediment transport and morphology. The flow module is based on solving the Reynold's averaged Navier-Stokes equations in the vertical plane with k-omega turbulence closure. The model has been extended to accept a general (but periodic) bottom boundary to be able to compare with field data. Boundary layer velocity profiles were measured using a Bistatic Coherent Doppler Velocity profiler (BCDV). A two-axis scanning sonar altimeter measured small-scale morphology over a 1 by 1.5 m area with 4 cm horizontal and 0.25 cm vertical resolutions. Bottom maps of small-scale morphology were obtained continuously every 20 minutes. A relatively simple data sequence was selected for model comparison, during which time the wave forcing evolved abruptly from  $H_{sig}=0.3m$  to  $H_{sig}=3.0m$  (bed velocity  $< 1$  m/s), and the bed evolved from no motion (relic) to actively migrating vortex ripples. SHOWEX bedform changes under low wave plus collinear current conditions resulted in minor changes of the vortex ripple fields. Bedform migration rates of the model were similar to the field migration rates. Like the field data, the modeled data under strong forcing removed smaller scale vortex ripples and redistributed the sediment into a larger scale ripple with a large portion of sediments in suspension above the bed. Limitations of the model owing to the 2-D assumption, periodic boundaries and monochromatic wave forcing constraints are discussed.

THIS PAGE INTENTIONALLY LEFT BLANK



## TABLE OF CONTENTS

<b>I.</b>	<b>INTRODUCTION.....</b>	<b>1</b>
<b>A.</b>	<b>MOTIVATION FOR STUDY.....</b>	<b>1</b>
<b>B.</b>	<b>OBJECTIVES.....</b>	<b>2</b>
<b>C.</b>	<b>BACKGROUND.....</b>	<b>3</b>
1.	Flow Properties .....	3
2.	Sediment Transport through the Shields Parameter.....	4
3.	Bedforms .....	4
4.	Numerical Solutions .....	5
<b>II.</b>	<b>DUNE2D MODEL FORMULATION.....</b>	<b>7</b>
<b>A.</b>	<b>FLOW MODULE.....</b>	<b>9</b>
1.	Conservation of Momentum and Mass .....	9
2.	Turbulent Kinetic Energy Equations using $\kappa\text{-}\omega$ Model.....	10
3.	Roughness of the Wall.....	11
<b>B.</b>	<b>SEDIMENT TRANSPORT.....</b>	<b>12</b>
1.	Bedload Calculations.....	14
2.	Suspended Load Calculations.....	15
<b>C.</b>	<b>MORPHOLOGY MODULE.....</b>	<b>17</b>
<b>D.</b>	<b>WAVE PLUS CURRENTS SUPPLEMENT.....</b>	<b>17</b>
<b>III.</b>	<b>FIELD DATA.....</b>	<b>19</b>
<b>A.</b>	<b>MEASUREMENTS.....</b>	<b>19</b>
<b>B.</b>	<b>VELOCITY FORCING AND BEDFORM MORPHOLOGY DURING 11-13 NOVEMBER 1999 .....</b>	<b>23</b>
<b>IV.</b>	<b>DUNE2D MORPHOLOGY OUTPUT ANALYSIS.....</b>	<b>27</b>
<b>A.</b>	<b>MODEL SENSITIVITY TESTS.....</b>	<b>27</b>
1.	Wave-only Case Study .....	28
2.	Wave plus Collinear Current Case Study.....	30
<b>B.</b>	<b>MODEL COMPARISON WITH SHOWEX '99 OBSERVATIONS .....</b>	<b>32</b>
1.	Simulation of Storm Event.....	32
2.	Discussion of Storm Event Simulation .....	37
<b>C.</b>	<b>WAVE SIMULATION OF FIELD STORM EVENT.....</b>	<b>40</b>
<b>V.</b>	<b>CONCLUSION .....</b>	<b>41</b>
	<b>APPENDIX A. DUNE2D MODEL SOLUTION .....</b>	<b>43</b>
<b>A.</b>	<b>MODEL INPUT.....</b>	<b>43</b>
1.	Hydrodynamic and Geophysical Input .....	43
2.	Numerics and Scheme Setup .....	44
3.	Grid Input .....	45
4.	Grid Sensitivity Study.....	47
5.	Model Boundary Conditions.....	47
6.	Sediment Transport Related Setup .....	48

7.	Morphology Setup.....	48
B.	MODEL OUTPUT .....	49
APPENDIX B. DUNE2D MODEL APPLICATION.....		51
A.	FORTRAN CODE FILES.....	51
B.	MODEL INITIATION FILES.....	52
1.	Input File.....	52
2.	Grid File .....	52
3.	Format File.....	52
4.	Summary .....	54
APPENDIX C. DUNE2D INPUT/OUTPUT TRANSFORMATION.....		57
A.	GENERAL I/O PROCEDURES.....	57
B.	FIELD DATA TRANSFORMATION.....	60
1.	Bedform Transformation.....	60
2.	Monochromatic Wave Dynamic Forcing Transformation .....	62
LIST OF REFERENCES .....		63
INITIAL DISTRIBUTION LIST.....		65

## LIST OF FIGURES

Figure 1.1.	Littoral Naval Interests. (after <a href="http://www.oc.nps.navy.mil/~stanton/miso/">www.oc.nps.navy.mil/~stanton/miso/</a> )	1
Figure 2.1.	DUNE2D Model Schematic Flow Diagram.	7
Figure 2.2.	Flow over a ripple bed.	8
Figure 3.1.	U.S. Army Corps of Engineers Field Research Facility at Duck, North Carolina. Site of SHOWEX 99. (from <a href="http://www.frf.usace.army.mil/">http://www.frf.usace.army.mil/</a> )	19
Figure 3.2.	SHOWEX 99 measurement platform location along Duck, N.C. (after <a href="http://cheyenne.rsmas.miami.edu/duck99/">http://cheyenne.rsmas.miami.edu/duck99/</a> ) The platform is approximately 1.4km off the beach.	20
Figure 3.3.	Bottom boundary layer measurement platform.	21
Figure 3.4.	Platform measurement orientation is 22° to the left of Beach North. Platform located in 11m depth.	22
Figure 3.5.	A two-dimensional bedform mapped using X-Y acoustic altimeter during SHOWEX '99. Black line is the BCDV measurement center. Right foreground is a hole generated by a live shellfish embedded in the ocean floor.	23
Figure 3.6.	FRF Duck, N.C. measured weather and oceanographic data from archived data collection for November 1999. Box indicates the storm event of 10-13 November. (after <a href="http://www.frf.usace.army.mil/">http://www.frf.usace.army.mil/</a> )	24
Figure 3.7.	Mean currents and oscillatory wave velocity amplitude for year days 315.5 to 316.6 illustrating storm event spin-up of the ocean dynamics.	25
Figure 3.8.	Evolution of bedform along centerline, cross-shore transect during storm event. (Positive x direction is towards the beach).	26
Figure 4.1.	Transformed cross-shore transect of bedform from SHOWEX '99 data (year day 315.9) used to initialize DUNE2D simulations. The beach is to the right with the initial oscillatory wave forcing going towards the right (See Appendix (C) for explanation of bedform transformation).	27
Figure 4.2.	DUNE2D bedform morphology for field bedform year day 315.9 with wave-only monochromatic forcing after 20 wave periods. (a) Test#1: $U_0=0.35\text{m/s}$ , $T=4.79\text{s}$ , $\psi=76$ ; (b) Test#2: $U_0=0.35\text{ m/s}$ , $T=10\text{s}$ , $\psi=76$ ; (c) Test#3: $U_0=0.70\text{m/s}$ , $T=4.79\text{s}$ , $\psi=303$ ; (d) Test#4: $U_0=0.70\text{m/s}$ , $T=10\text{s}$ , $\psi=303$ .	29
Figure 4.3.	DUNE2D bedform morphology given an initial bedform (field year day 315.9) with monochromatic wave ( $U_0=0.35\text{m/s}$ , $T=4.8\text{s}$ , $\psi=76$ ) plus current forcing after 20 wave periods. (a) Test#5: $U_c/U_0=0.5$ ; (b) Test#6 $U_c/U_0=1.0$ ; (c) Test#7: $U_c/U_0=2.0$ ; (d) Test#8: $U_c/U_0=-2.0$ .	31
Figure 4.4.	Test#9: DUNE2D morphology time series given an initial bedform (year day 315.9) with low wave energy ( $U_0=0.16$ , $T=4.8$ , $U_c=-.11$ , $\psi=16$ , $A=0.12\text{m}$ ).	35
Figure 4.5a.	Test #9: DUNE2D morphology bedform snapshots over simulation time resulting in a vortex ripple field at equilibrium state (ripple geometry:	

	$\lambda_{Avg}=0.11m$ , $\eta_{Avg}$ (height) = 0.02m, $\eta_{Avg} / \lambda_{Avg}$ (slope) = 0.18, $\lambda_{Avg}/A=0.92$ ). Migration: 4.2cm/hr onshore.....	35
Figure 4.5b.	SHOWEX '99 Bedform morphology time series snap shots taken from year day 315.9 to 2.4 hours later. (superimposed vortex ripple geometry: $\lambda_{Avg}=0.2m$ , $\eta_{Avg} = 0.008m$ , $\eta_{Avg} / \lambda_{Avg} = 0.04$ ) Migration: 4.5cm/hr onshore.....	35
Figure 4.6.	Test#10: DUNE2D morphology time series given an initial bedform (year day 315.9) with high wave energy ( $U_o=0.74$ , $T=9.6$ , $U_c=-0.1$ , $\psi=341$ , $A=1.1m$ ).....	36
Figure 4.7a.	Test #10: DUNE2D Model morphology bedform snapshots over simulation time resulting in a flat mega-ripple equilibrium state (ripple geometry: $\lambda_{Average}=1.8m$ , $\eta = 0.008m$ , $\eta/\lambda = 0.005$ , $\lambda_{Average}/A= 1.5$ ).....	36
Figure 4.7b.	SHOWEX '99 Bedform morphology time series snap shots taken from year day 316.4 (bedform during peak wave forcing) to 3.6 hours later. (Ripple geometry: $\lambda_{Average}=1.5m$ , $\eta = 0.02m$ , $\eta/\lambda = 0.02$ ). Migration: 2.2 cm/hr on-shore.....	36
Figure 4.8.	DUNE2D initial bedform for (a)Test #11,(b) Test #12, (c) Test #13 (d) Test #14.....	38
Figure 4.9.	DUNE2D morphology simulations illustrating bedform evolution at equilibrium (+2.6hrs) for (a)Test #11( $\lambda_{Avg}=1.8m$ ), (b) Test #12 ( $\lambda_{Avg}=2.2m$ ), (c) Test #13 ( $\lambda_{Avg}=1.5m$ ). (d) Test#14 (unresolved $\lambda_{Avg}$ ).....	39
Figure A.1.	DUNE2D grid using the transfinite interpolation method.....	46
Figure B.1.	DUNE2D input/output flow diagram.....	55
Figure C.1.	General input/output flow diagram of modeling simulation.....	57
Figure C.2.	DUNE2D input data flow of MATLAB programs.....	58
Figure C.2.	DUNE2D output data flow of MATLAB programs.....	59
Figure C.3.	MATLAB programs used to transform field data into model input.....	60
Figure C.4.	Transformation of cross-shore field bedform data to DUNE2D non-dimensional bedform data.....	61

## LIST OF TABLES

Table 4.1.	Four test cases in wave-only sensitivity study of morphology simulations....	28
Table 4.2.	Model hydrodynamic input for wave plus current sensitivity study of morphology simulations.....	30
Table 4.3.	Two test cases in storm event case study of morphology simulations. ....	34
Table 4.4.	Storm event ripple geometry comparison (DUNE2D vs. SHOWEX) .....	37
Table 4.5.	Grid test cases to verify boundary effects on morphology simulations.....	38
Table A.1.	Hydrodynamic and geophysical input. ....	44
Table A.2.	Numerical Input.....	45
Table A.3.	Grid Input.....	46
Table A.4.	Grid Sensitivity of the Flow Test Results.....	47
Table A.5.	Sediment Transport Input. ....	48
Table A.6.	Morphology Input.....	49
Table A.7.	Morphology Mode Output. (Period Average Mean). ....	50
Table B.1.	Fortran DUNE2D Files. {Program areas: a)I/O: input/output b)F: flow c)S: sediment transport d)M: morphology e)G/B: grid/boundary} .....	51
Table B.2.	Files necessary for simulation. (*user option, not required).....	55

THIS PAGE INTENTIONALLY LEFT BLANK

## ACKNOWLEDGMENTS

The author would like to gratefully acknowledge the support and advice of Dr. Edward B. Thornton, Dr. Timothy P. Stanton, Dr. Diane Foster, and Dr. Ken Andersen. Without their dedication to research in their field of science this work would not have been possible. The author wants to recognize and appreciate the financial support of the Office of Naval Research for this work.

Finally, the author would like to thank his wife, Denise, and son, Jack, for their unconditional support, patience, and understanding throughout this entire thesis.

THIS PAGE INTENTIONALLY LEFT BLANK

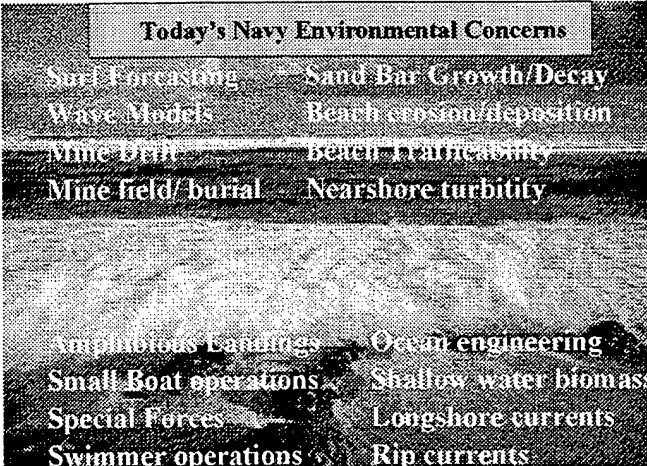


## I. INTRODUCTION

This is a study of ripple migration, evolution, and erosion on the inner continental shelf over time. Despite several decades of analytical and empirical research, understanding the evolution of bedform morphology remains a fairly young field. In this thesis, the morphology problem is considered for non-breaking waves in the shallow-to-intermediate water depth range of the inner shelf. Current research emphasis is placed on numerical simulation of this problem. This chapter provides motivation for study, research objectives, and background on the bottom boundary layer with emphasis on the interactions of hydrodynamic forcing on sediment transport and bedforms.

### A. MOTIVATION FOR STUDY

Naval operations have rapidly transitioned from "blue", open ocean into coastal, shallow and intermediate waters. The operational oceanographer is required to implement ocean models of the littoral region to produce accurate forecasts of ocean processes. Figure (1.1) lists some Navy operations, as well as dynamic processes that are of concern.



Today's Navy Environmental Concerns	
Surf Forecasting	Sand Bar Growth/Decay
Wave Models	Beach erosion/deposition
Mine Drill	Beach Trafficability
Mine field/burial	Nearshore turbidity
Amphibious Landings	Ocean engineering
Small Boat operations	Shallow water biomass
Special Forces	Longshore currents
Swimmer operations	Rip currents

Figure 1.1. Littoral Naval Interests. (after [www.oc.nps.navy.mil/~stanton/miso/](http://www.oc.nps.navy.mil/~stanton/miso/))

Over the past decade, naval research has been highly focused on adapting to this new theater of operation. Field studies, laboratory experiments, and numerical modeling research of these highly spatial and temporal varying processes are motivation to improve physical understanding of the waves, currents, sediment transport, and bottom morphology in the littoral region. Advances are slow and expensive. Hopefully, the knowledge gained through the combined observations and simulation of the nearshore environmental processes will provide accurate oceanographic forecasts for required operational applications.

Common to all dynamic processes in the littoral region are the hydrodynamic forces produced through wave, current, and tidal energy. Motivation for this thesis is based on understanding wave and current interactions with the bottom boundary layer that force sediment transport in the form of bedload and suspended load, and result in bedform evolution and migration.

Wave-formed ripples are the dominant bedforms in coastal regions (Traykovski, et al, 1999). Over time, mobile beds can evolve in such a way that the overall bed roughness is changed. Furthermore, migration of sediment affects form drag on the existing hydrodynamic processes, net sediment transport, and the bottom boundary layer turbulence generation. These changes can have significant affect on wave energy dissipation (Ardhuin, 2000).

## **B. OBJECTIVES**

The objective is to simulate the migration and evolution of small-scale bedforms measured in the field using DUNE2D, a numerical model of the bottom boundary layer for small-scale morphology. The model is initiated using bedform and velocity

measurements acquired during the SHOWEX field experiment conducted from September to December 1999 at Duck, North Carolina. Small-scale bottom maps and high-resolution velocity measurements of a specific storm event are used to qualitatively verify DUNE2D output. Efforts are focused on simulating actual field conditions from an initial bed configuration. The long-term objective is to provide model validation to enhance numerical prediction of nearshore processes, particularly to predict ripple formation and migration.

## **C. BACKGROUND**

### **1. Flow Properties**

Accurately determining the flow field in the bottom boundary layer is essential to predicting sediment transport and morphology evolution. Flow in the ocean is by nature turbulent. Sediment transport calculations require estimates of the bed stress,  $\tau_b$ ,

$$\tau_b = \rho u_*^2 \quad (1.1)$$

where the shear stress is proportional to the frictional velocity,  $u_*^2$ . Flow field dynamics are complicated by irregular waves. In the inner shelf regions, flow near the bed is influenced by wave groupiness. Quantitative representation is made difficult through multiple wave packets interacting with each other superimposed with mean currents of varying strength and direction. Deigaard *et al* (1999) found net sediment transport under regular waves and wave groups with bound long waves to be dependent on sediment size, as well as wave characteristics.

## 2. Sediment Transport through the Shields Parameter

Sediment transport can be described in terms of the Shields parameter. The Shields parameter is the ratio of the destabilizing forces of the bottom stress and the stabilizing force of gravity acting on the sediment,

$$\theta = \frac{\tau_b}{\rho g(s-1)d} \quad (1.2)$$

where  $g$  is the gravitational acceleration,  $d$  is the sediment diameter, and  $s$  is the ratio of sediment density to fluid density. Sediments have a critical shear stress that is dependent upon their grain size, density, porosity, and shape. Once the shear stress exceeds this critical threshold, the viscous sub-layer breaks down, and the sand grains are set in motion. As the strength of the flow increases, the grains are lifted off the bed. As long as the settling velocity of the sediment is small compared with the forces producing lift, the grains will remain in suspension above the bed. The grains redistribute back to the bed when the fluid forces acting on the grains become less than the gravitational forces. Deposition is difficult to predict, as the flow field has eddies of varying strength and size. For high Shields numbers ( $\theta > 1$ ) under non-breaking waves, Diegard *et al* (1999) found that sheet flow occurs, where a large portion of the bedform sediment is set into motion, such that the remaining bed is planar in shape. For forcing with low Shields numbers, ripple-dominated bedforms occur.

## 3. Bedforms

Ripples are classified by their geometry and commonly divided into two separate spatial scales. Dunes, antidunes, megaripples and relic ripples are considered large-scale bedforms. Small-scale ripples include vortex, cross-ripples and rolling grain ripples.

Small-scale ripples are categorized by a length of less than 0.6 meters and a height roughly ten percent of the length, or below 0.06 meters (Engelund and Fredsoe, 1982).

Bagnold (1946) described two types of wave-induced ripples: rolling grain and vortex ripples. For increasing Shields numbers, as the critical value is just exceeded for flow over a flat, sandy seabed, grains oscillate back and forth in a rolling motion. This condition is difficult to find in nature (Andersen, 1999). As the flow intensity increases and the turbulent eddies induce more sediment transport, the oscillatory wave action organizes the moving grain into the classic vortex ripple triangular shapes. Over time, the sediment is moved from the trough of the ripple, and deposited through bedload and suspended load towards the ripple peak. The steepness of the ripple increases. Eventually, the flow vortex, formed by the fluid moving over the ripple peak, separates from the bed and induces further sediment transport (Neilsen, 1981). Many studies have been conducted to find equilibrium or quasi-equilibrium forms of the bed due to wave and current forcing with the objective of predicting ripple wavelength, height, and steepness as a function of mobility number or Shields parameter.

#### **4. Numerical Solutions**

Several numerical approaches have been used to describe the flow in the bottom boundary layer over an arbitrary bedform. Perrier's (1996) discrete vortex (DV) method does a good job describing the qualitative features of the flow. Turbulence models provide better quantitative description, which is required for morphological calculations (Andersen, 1999). The  $\kappa$ - $\epsilon$  turbulence closure technique was used by Sato (1986), Tsujimoto *et al.* (1991), and Perrier (1996), while Wilcox (1988, 1993b) introduced the

$\kappa$ - $\omega$  turbulence closure. The  $\kappa$ - $\omega$  model handles the strong pressure gradients near the separation point of the turbulent eddies better than the  $\kappa$ - $\epsilon$  model.

The present DUNE2D model study uses the  $\kappa$ - $\omega$  closure. The model is presented in the next chapter. Good results have been obtained by Andersen (1999) using DUNE2D for monochromatic wave and wave plus current forcing compared with laboratory data (Fredsoe *et al.*, 1999).

## II. DUNE2D MODEL FORMULATION

DUNE2D is a bottom boundary layer model for sediment transport over small-scale ripple morphology (Andersen, 1999). The model resolves two-dimensional flow over a one-dimensional bedform. DUNE2D is a modular Fortran code, which evolved over many years of research on flow, sediment transport, and most recently, morphology at the Technical University of Denmark. DUNE2D is composed of three modules: flow, transport, and morphology. A flow diagram of the model is represented in Figure (2.1).

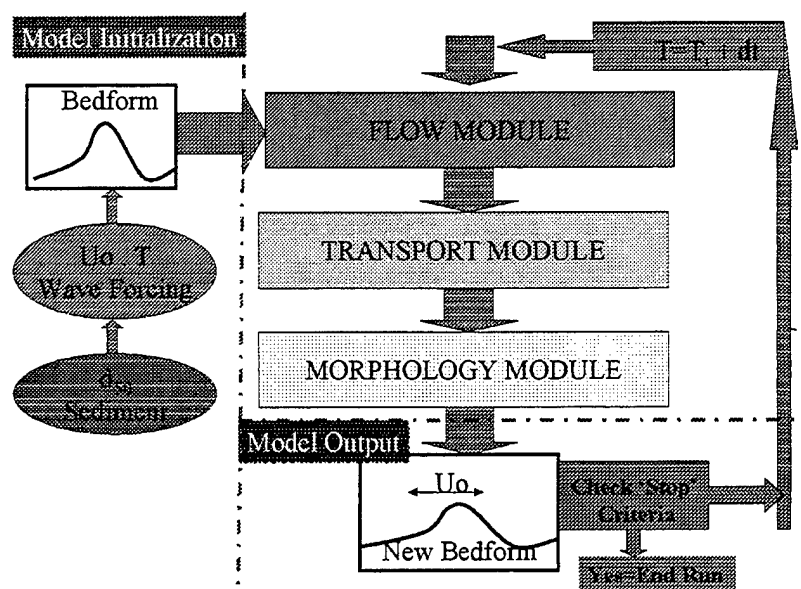


Figure 2.1. DUNE2D Model Schematic Flow Diagram.

The program has several modes of simulation. For each mode, several physical assumptions and numerical modeling techniques exist. The model can be run for flow and sediment transport simulations, or for bottom boundary layer flow alone. For purposes of this study, systematic solutions for all three principle modules are considered with emphasis on the evolution of bedforms. Therefore, the model description in this chapter will be presented from a morphology simulation perspective.

Dynamic forcing is through periodic, sinusoidal wave input. If desired, a mean along-axis current can be included. At each grid point of the model, the horizontal,  $u$ , and vertical,  $w$ , velocity flow components are evaluated. Flow solutions are passed to the transport module where sediment characteristics, as well as the flow solutions, influence sediment transport calculations. Strong turbulent flow is capable of sediment transport, both along the bed and in suspension above the bed. Transport solutions are passed to the morphology module where bedform changes are integrated over time.

DUNE2D models oscillatory flow with an optional mean collinear current over a rippled bedform, as illustrated by Figure (2.2). The twelve parameters listed in Figure (2.2) are required to describe the model domain. Appendix (A) provides a further explanation of the input parameters. Hydrodynamic forcing, geophysical properties of the sediment, numerical schemes, grid definitions, boundary conditions, transport methods, and morphology setup are some of the categories that are used to describe model input. Appendix (B) provides examples of the ASCII input files and the procedural method used to implement DUNE2D code.

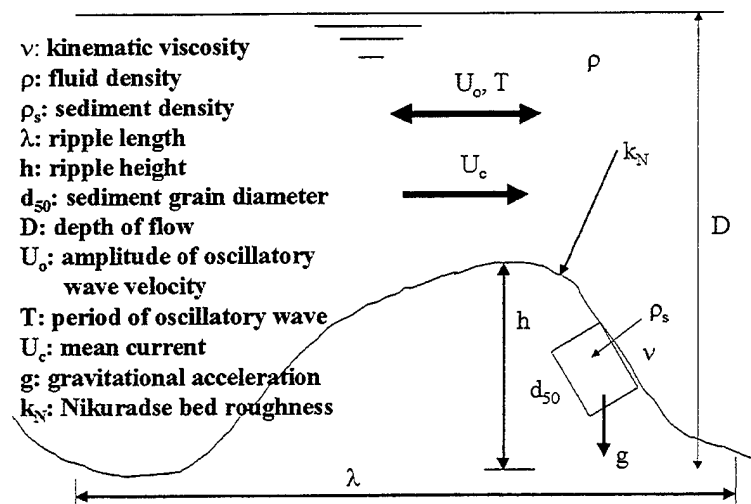


Figure 2.2. Flow over a ripple bed.



## A. FLOW MODULE

The flow module models fully turbulent flows, with Reynolds numbers ranging between  $10^5$  to  $10^6$ , in the bottom boundary layer. The model initializes input variables and sets necessary default values, and then solves the flow field given specific dynamic forcing over an arbitrary one-dimensional bedform.

### 1. Conservation of Momentum and Mass

The two-dimensional flow equations along the horizontal and vertical axis assume an incompressible, Newtonian fluid. The conservation of momentum is,

$$\frac{\partial u_i}{\partial t} + u_j \frac{\partial u_i}{\partial x_j} = -\frac{1}{\rho} \frac{\partial p}{\partial x_i} + 2\nu \frac{\partial}{\partial x_i} \left( \frac{1}{2} \left( \frac{\partial u_i}{\partial x_j} + \frac{\partial u_j}{\partial x_i} \right) \right) \quad i, j = 1, 2 \quad (2.1)$$

where  $p$ ,  $u_i$ ,  $\rho$ , and  $\nu$  represent pressure, velocity, density and kinematic viscosity, respectively. The continuity equation is described by,

$$\frac{\partial u_i}{\partial x_i} = 0 \quad i = 1, 2 \quad (2.2)$$

The Reynolds-averaged Navier-Stokes (RNS) momentum equations are obtained by applying Reynolds decomposition and averaging to Equations (2.1) and (2.2) with the pressure and flow quantities divided into a mean and fluctuating components (e.g.  $u_i = U_i + u_i'$ ).

$$\frac{\partial U_i}{\partial t} + U_j \frac{\partial U_i}{\partial x_j} = -\frac{1}{\rho} \frac{\partial P}{\partial x_i} + 2\nu \frac{\partial}{\partial x_i} \left( \frac{1}{2} \left( \frac{\partial U_i}{\partial x_j} + \frac{\partial U_j}{\partial x_i} \right) \right) - \frac{\partial}{\partial x_j} \left( \overline{u_j' u_i'} \right) \quad (2.3)$$

$$\frac{\partial U_i}{\partial x_i} = 0 \quad (2.4)$$

where the mean component resolves the waves and currents, denoted by a capital letter, the turbulence fluctuations are denoted by primes, and the over bar indicates time averaging. A slow time variation of the mean velocity is allowed.

The last term in Equation (2.3) is the Reynolds stress tensor. The RNS equations are closed using turbulent viscosity closure, where the stress tensor is modeled as

$$-\overline{u'_j u'_i} = \nu_T \frac{\partial \left( \frac{1}{2} \left( \frac{\partial U_i}{\partial x_j} + \frac{\partial U_j}{\partial x_i} \right) \right)}{\partial x_j} - \frac{2}{3} k \delta_{ij} \quad (2.5)$$

$$\text{where } k = \frac{1}{2} \overline{(u'^2 + w'^2)}$$

$\nu_T$  is the turbulent viscosity and  $\delta_{ij}$  is the Kronecker delta. Equation (2.5) describes a dampening and diffusion process.

## 2. Turbulent Kinetic Energy Equations using $\kappa$ - $\omega$ Model

A two-equation  $\kappa$ - $\omega$  model is used to determine eddy viscosity as a function of time and space (Anderson, 1999). The  $\kappa$ - $\omega$  model (Wilcox (1988; 1993b)) was selected over the more commonly used  $\kappa$ - $\epsilon$  model to accommodate boundary conditions on a rough bed in unsteady flow with strong pressure gradients along the bottom boundary. The turbulent viscosity term in Equation (2.5) has a direct relationship to  $\kappa$  (kinetic energy) and  $\omega$  (vorticity) through a model constant  $\gamma^*$ .

$$\nu_T = \gamma^* \frac{\kappa}{\omega} \quad (2.6)$$

The turbulent kinetic energy equations are used to solve for  $\kappa$  and  $\omega$ . (Wilcox, 1993b)

$$\frac{\partial \kappa}{\partial t} + U_j \frac{\partial \kappa}{\partial x_j} = \frac{\partial}{\partial x_j} \left[ (\nu + \sigma \nu_T) \frac{\partial \kappa}{\partial x_j} \right] - \overline{u_i u_j} \frac{\partial U_i}{\partial x_j} - \beta^* \kappa \omega \quad (2.7)$$

$$\frac{\partial \omega}{\partial t} + U_j \frac{\partial \omega}{\partial x_j} = \frac{\partial}{\partial x_j} \left[ (\nu + \sigma \nu_T) \frac{\partial \omega}{\partial x_j} \right] + \gamma \frac{\omega}{\kappa} \left( -\overline{u_i u_j} \frac{\partial U_i}{\partial x_j} \right) - \beta \omega^2 \quad (2.8)$$

where closure coefficients :  $\gamma^* = 1$ ;  $\gamma = \frac{5}{9}$ ;  $\beta^* = \frac{9}{100}$ ;

$$\beta = \frac{3}{40}; \quad \sigma = \frac{1}{2}; \quad \sigma^* = \frac{1}{2}$$

These equations are similar to the  $\kappa$ - $\varepsilon$  model, where  $\varepsilon$  is the local dissipation rate of turbulent kinetic energy. The term  $\omega$  does not have a direct physical meaning, but can be described as the vorticity of turbulent eddies (Saffmen, 1970), and is related to  $\varepsilon$  by,

$$\varepsilon = \beta^* \kappa \omega \quad (2.9)$$

### 3. Roughness of the Wall

The bottom boundary is scaled using the concept of a rough wall through the Nikuradse roughness,  $k_N/30$ . In DUNE2D,  $k_N$  is set to two and a half times the median grain diameter. (Fredsoe and Diegaard, 1992).

$$k_N = 2.5 d_{50} \quad (2.10)$$

The law of the wall is applied to the bottom boundary condition associated with the sandy bed. A modification is made to a smooth wall to fit the empirically rough wall solution. (Andersen, 1999). The bottom boundary condition is a no-slip condition for the

flow, which implies a viscous sub-layer and  $\kappa=0$  at the bed, while  $\omega$  follows (Wilcox, 1993b):

$$\omega = \frac{U_f^2 S_R}{\nu} \quad (2.11)$$

$$\text{where } U_f = \text{friction velocity} = \sqrt{\frac{\tau_{wall}}{\rho}} \quad (2.12)$$

$$S_R = \begin{cases} (50/k_N^+)^2, & k_N^+ z < 25 \\ (100/k_N^+), & k_N^+ z \geq 25 \end{cases}$$

Andersen states that the methodology for attaining a rough wall solution through parameterization constant,  $S_R$ , is not physically correct. Wall functions are normally used with turbulent kinetic energy models that don't involve viscous sub-layers. The  $\kappa$ - $\omega$  model has a viscous sub-layer due the no-slip condition imposed at the bottom boundary. Andersen also points out that model results using the  $\kappa$ - $\omega$  model are sensitive to the free-stream boundary condition for  $\omega$ . To overcome this problem, a symmetric boundary is applied to the upper boundary. (Andersen, 1999)

## B. SEDIMENT TRANSPORT

DUNE2D separates sediment transport into bedload and suspended load calculations using techniques described by Engelund and Fredsoe (1976) and Fredsoe and Diegaard (1992). Turbulent flow causes destabilizing forces upon the rippled bed. Sediment is thrown into motion when strong destabilizing forces, specifically, drag and lift, overcome gravitational stabilizing forces. Segregation of bedload and suspended load is imposed by an imaginary boundary. Moving sediment in repeated contact with

the bed is known as bedload transport. Suspended load transport is sediment in motion above the bedload transport boundary, defined at a height  $2d$ , by a function

$$c_b(\theta, \gamma) \Big|_{z=2d} \quad (2.13)$$

where  $\theta$  is the Shields parameter and  $\gamma$  is the slope of the bed and  $d$  is the median grain diameter. Both transport load calculations are based on the Shields parameter,  $\theta'$ , for a flat bed (Equation 1.2), where the maximum shear stress during a wave cycle is

$$\tau'_b = \frac{1}{2} \rho f_w U_o^2 \quad (2.14)$$

where  $U_o$  is the wave velocity amplitude and the wave frictional coefficient is,

$$f_w = 0.04 \left( \frac{A}{k_N} \right)^{-0.25}, \quad \frac{A}{k_N} > 50 \quad (2.15)$$

where  $A$  is the orbital amplitude of the wave motion,

$$A = \frac{U_o T}{2\pi} \quad (2.16)$$

The local bed shear must be greater than the critical bed shear for sediment motion to be initiated. Bedload is a function of the bed shear, while suspended load is a function of bed shear as well as settling velocity. The settling velocity of the sediment is determined using an empirical formula for the drag coefficient of sand (Fredsoe and Deigaard, 1992):

$$w_s = \sqrt{\frac{4(s-1)gd}{3C_D}} \quad (2.17)$$

$$C_D = 1.4 + \frac{36}{\text{Re}_d}; \quad \text{Re}_d = \frac{w_s d}{\nu}$$

where  $C_D$  is the drag coefficient and  $Re_d$  is the sediment Reynolds number.

### 1. Bedload Calculations

Bedload calculations are based on the Engelund and Fredsoe (1976) formulation. Sediment velocity is found from the balance of the gravity, drag, and friction forces on a single grain on a sloping bed. The non-dimensional single grain velocity is given by,

$$\frac{U_b}{U_f} = \alpha \left( 1 - 0.7 \sqrt{\left| \frac{\theta_{cy}}{\theta} \right|} \right); \quad \alpha = 10 \text{ (empirical constant);} \quad (2.18)$$

where  $U_b$  is the grain velocity and  $\theta_{cy}$  is the critical Shields number for a sloping bed,

$$\theta_{cy} = \theta_c \left( \sigma \cos \gamma + \frac{\sin \gamma}{\mu_D} \right) \quad (2.19)$$

in which  $\sigma$  is the sign of the direction of the bed load and the critical Shields parameter for a flat bed is,

$$\theta_c = \frac{4\mu_D}{3C_D\alpha^2}$$

for which  $\mu_D$  is the dynamic friction coefficient. (Andersen, 1999)

It is assumed only a single layer of grains can be in motion at the bed. From this assumption, an equation, based on empirical data, is used to solve the fraction of grains that are in motion per unit area,

$$n = \frac{1}{d^2} \left[ 1 + \left( \frac{\frac{\pi}{6} \mu_d}{\theta' - \theta_c} \right)^4 \right]^{-0.25} \quad (2.20)$$

Knowing the number, or probability of grains in motion, bedload transport, or bedload flux, the rate of transport of a volume of sediment per time, is determined. The non-dimensional bedload flux is (Fredsoe and Diegaard, 1992)

$$\phi_b(\theta, \gamma) = n \frac{\pi}{6} d^3 U_b \sqrt{(s-1)gd^3} \quad (2.21)$$

After substituting for  $n$ ,  $U_b$ , and including Fredsoe's linear gravity correction to the Meyer-Peter flat bed equation for bedload flux, Equation (2.21) simplifies to:

$$\phi_b(\theta, \gamma) = 8(\theta - \theta_c - \beta\gamma)^{1.5} \quad (2.22)$$

where  $\beta = 0.1$ .

## 2. Suspended Load Calculations

Suspended sediment is advected by wave motion and mean currents while falling towards the bed based on the sediment's settling velocity,  $w_s$ . Strong turbulent fluctuations with small settling velocity sediment produce sediment in suspension above the bedload boundary. Suspended sediment concentration,  $c$ , is modeled by,

$$c = c_0 \left( 1 + \frac{1}{\lambda_f} \right)^{-3}; \quad c_0 = 0.65 \text{ gm}^{-3} \quad (2.23)$$

where  $\lambda_f$ , the mean free path of the sediment at the bedload boundary condition, is

$$\lambda_f^2|_{z=2d} = \frac{4\kappa^2}{0.013 \rho s \theta} \left( \theta - \theta_{cy} - n \frac{\pi}{6} d^2 \mu_d \right) \quad (2.24)$$

and  $n$ , again, represents the fraction of grains in motion per unit area as described by Equation (2.20).

The total instantaneous suspended concentration is found using Equation (2.23) where the time rate change of concentration is calculated using a transport-diffusion equation:

$$\frac{Dc}{Dt} = w_s \frac{\partial c}{\partial z} + \nabla(\varepsilon_s \nabla c) \quad (2.25)$$

where the settling velocity is represented by  $w_s$  using Equation (2.17) and the term  $\varepsilon_s \approx \nu_T$  is the suspended sediment diffusivity, which is equal to the eddy viscosity defined by Equation (2.6).

The instantaneous suspended sediment flux is obtained through the instantaneous velocity distribution and concentration found from Equation (2.25),

$$q_s = u(x, z, t)c(x, z, t) \quad (2.26)$$

Finally, The total sediment load flux,  $q_t$ , through a cross section, is the vertical integral of the flux profile,

$$q_t(x, t) = q_b(x, t) + \int_{h(x, t)}^D q_s(x, z, t) dz \quad (2.27)$$

Andersen states that one of the fundamental problems with the calculation of the bedload transport is that it is based on mean bed shear stresses. The model does not incorporate the turbulent fluctuations,  $\kappa$ . Despite this deficiency, dynamic ripple mechanisms are preserved. (Andersen, 1999)



### C. MORPHOLOGY MODULE

The morphology module is based on the continuity of mass for sediment. From the total transport Equation (2.27), the change of the bedform over time is found by time integrating,

$$\frac{\partial h(x,t)}{\partial t} = -\frac{1}{1-p} \frac{\partial q_t(x,t)}{\partial x} \quad (2.28)$$

where  $p$  is the porosity of the sand. The main interest for the morphology simulations is the mean bed height at the end of each wave period. For further discussion of the output parameters see Appendix (A).

### D. WAVE PLUS CURRENTS SUPPLEMENT

The model forcing can be supplemented with the addition of a collinear current on the oscillatory flow. The addition of the current is made through a replacement of the constant friction factor for wave-only flows to a wave plus current friction factor,  $f_{wc}$ ,

$$f_{wc} = 2 \left( \frac{U_f D}{Q} \right)^2 \quad (2.29)$$

where  $f_{wc}$  is the constant friction factor for the current in a wave plus current flow.  $D$  is the depth scaling term and  $Q$  is the water discharge per unit width (Fredsoe et al., 1999).

An equivalent Nikuradse roughness,  $k_{wc}$ , is related to  $f_{wc}$  by

$$k_{wc} = 14.8 D \exp \left( \frac{-0.57}{\sqrt{f_{wc}}} \right) \quad (2.30)$$

The advection of sediment by the mean flow is calculated in the bedload and suspended load modules.

THIS PAGE INITIALLY LEFT BLANK

### III. FIELD DATA

A long-term inner shelf study of the bottom boundary layer was part of the Shoaling Waves Experiment, SHOWEX, at Duck, North Carolina (Figure 3.1). Multi-scale measurements of the hydrodynamic interactions over sandy rippled bedforms were made. This chapter describes the data collection procedure, measurement techniques, and bedform morphology due to ocean forcing caused by a specific storm event.

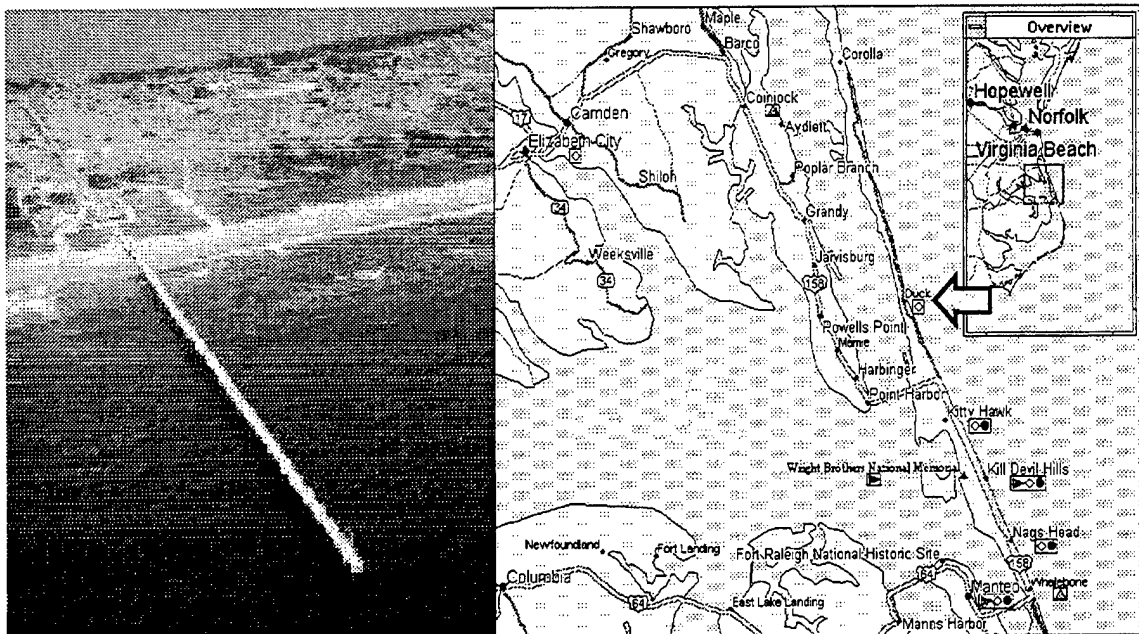


Figure 3.1. U.S. Army Corps of Engineers Field Research Facility at Duck, North Carolina. Site of SHOWEX 99. (from <http://www.frf.usace.army.mil/>)

#### A. MEASUREMENTS

SHOWEX was an Office of Naval Research funded Directed Research Initiative (DRI) to improve wave propagation models in the coastal regions. One of the objectives was to measure the dissipation of shoaling waves across the inner shelf with emphasis on the affects of the feedback between wave induced ripples and the resulting increased

dissipation of the waves at the bed. Measurements of the bottom boundary layer were made at 11 meters water depth from a bottom mounted platform with precision instruments at site S-3 (Figure 3.2) at Duck, North Carolina, during 28 September to 10 December 1999.

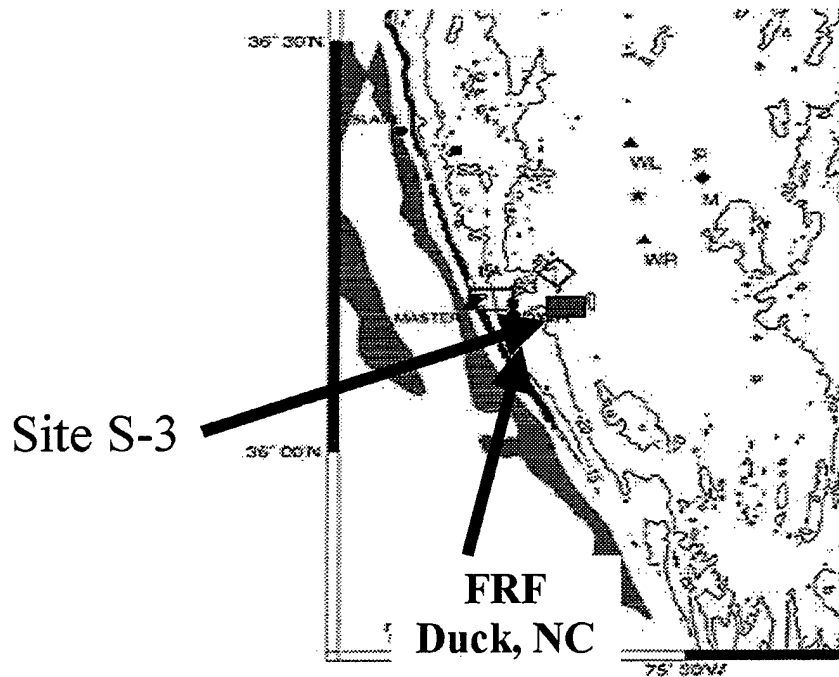


Figure 3.2. SHOWEX 99 measurement platform location along Duck, N.C. (after <http://cheyenne.rsmas.miami.edu/duck99/>) The platform is approximately 1.4km off the beach.

Sediment collection of the relatively homogeneous fine sand was made in the observation area four times during the three-month experiment. The median sediment diameter was 0.1 mm based on a sieving procedure.

A schematic representation of the instrument platform is shown in Figure (3.3), illustrating the sensors used to measure velocities within the bottom boundary layer as well as the bedform and suspended sediment concentrations. A 1.3 MHz pulsed, bistatic

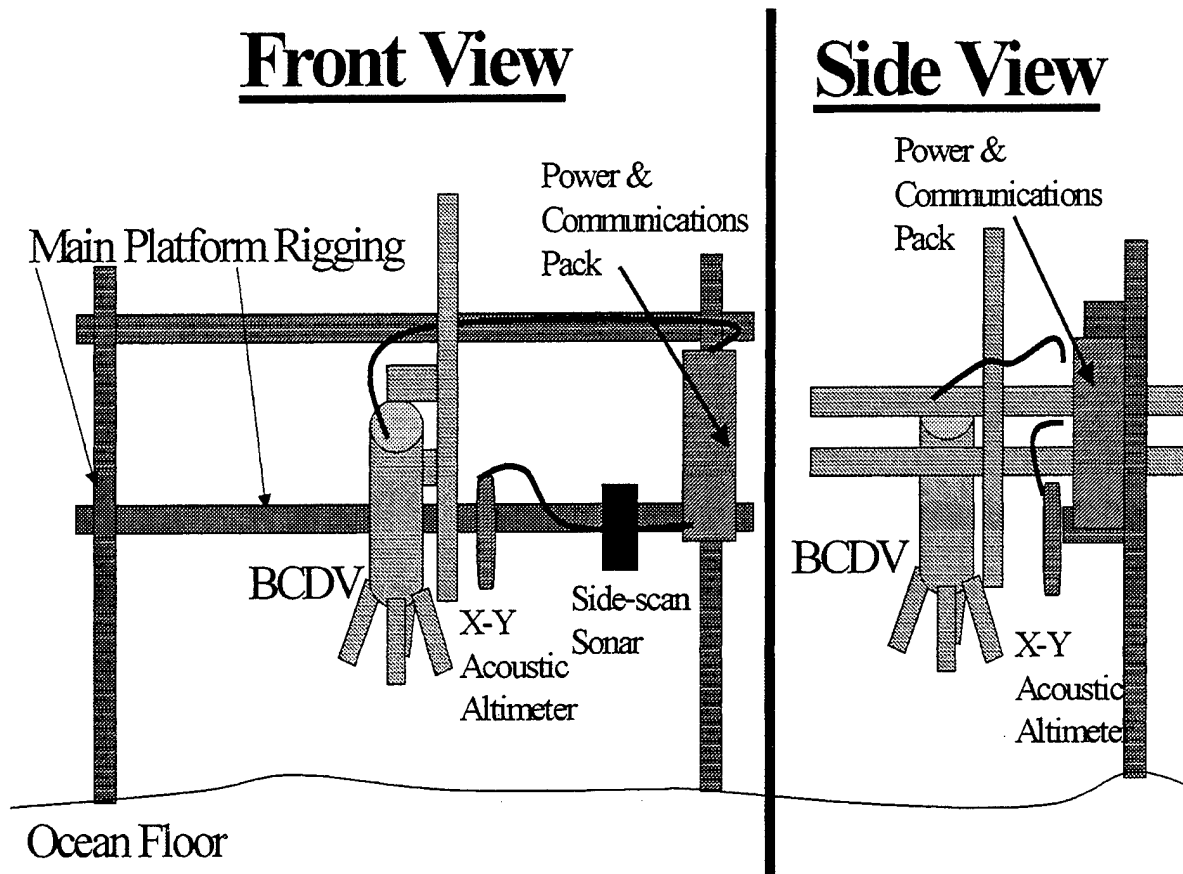


Figure 3.3. Bottom boundary layer measurement platform.

coherent Doppler velocity (BCDV) profiler (Stanton 1996, 2000) measured vertical profiles of three component velocities,  $u$ ,  $v$ , and  $w$ , and sediment concentration in 2 cm diameter volumes of water every 0.6 cm over the bottom 60 cm, starting at 30 cm from the sensor face. The sampling frequency was 18Hz, resulting in high resolution velocity profiles. The BCDV's orientation is illustrated in Figure (3.4). Tilt sensors in the BCDV allowed precise orientation of the vertical coordinate system. The raw BCDV vector velocity profile data were transformed into an earth-referenced coordinate system during post-processing.

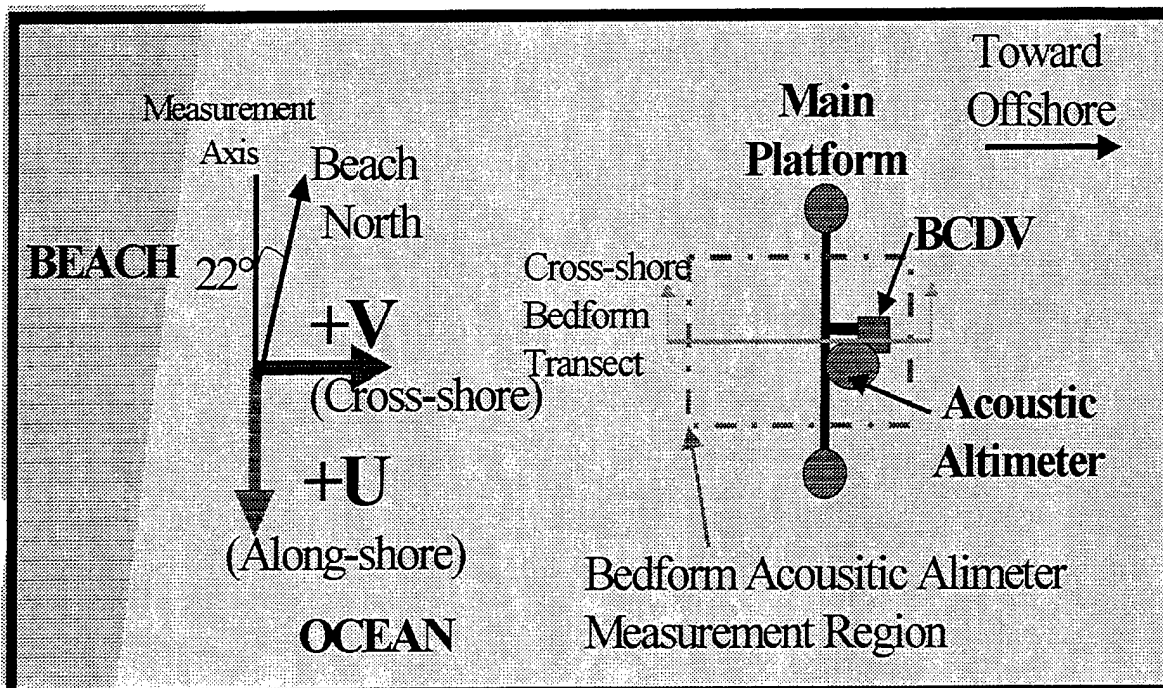


Figure 3.4. Platform measurement orientation is 22° to the left of Beach North. Platform located in 11m depth.

A two-axis, scanning, high-resolution acoustic altimeter was collocated with the BCDV profiler on the instrument platform. The scanning altimeter mapped a 4m by 2m bed area every 15 to 30 minutes. Resolution of the bed was 4cm in the horizontal and 0.25 cm in the vertical over an inner 1 m<sup>2</sup> area. Horizontal resolution decreases away from the measurement center due to steep sensor angles and distances of travel. Post-processing of the raw range data included removal of false targets, transformation of range and tilt angles into Cartesian coordinates, and objective analysis techniques to smoothly map the scanned data points across the measurement area. Final bedform observation boundary limits, shown in Figure (3.5), were reduced to 1.5m by 1m box defining an area of maximum resolution.

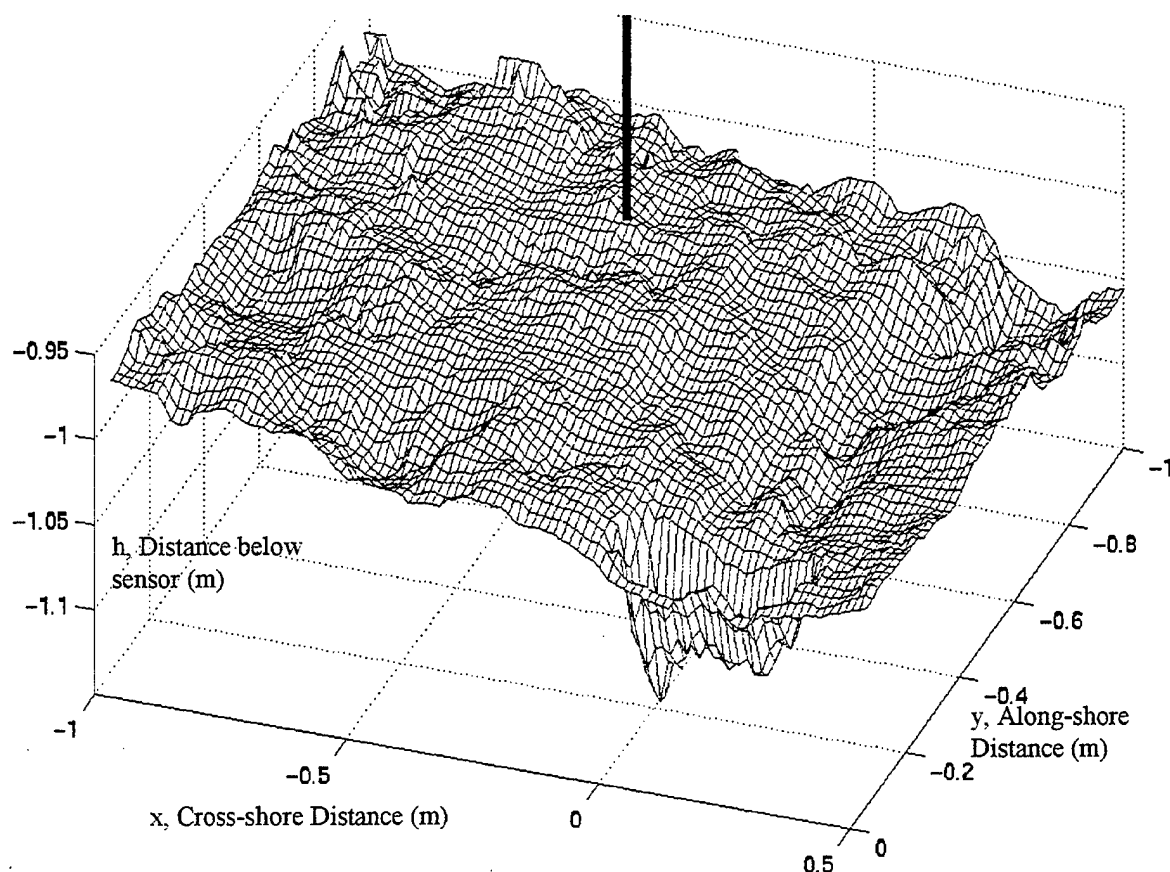


Figure 3.5. A two-dimensional bedform mapped using X-Y acoustic altimeter during SHOWEX '99. Black line is the BCDV measurement center. Right foreground is a hole generated by a live shellfish embedded in the ocean floor.

## B. VELOCITY FORCING AND BEDFORM MORPHOLOGY DURING 11-13 NOVEMBER 1999

The evolution and migration of bedform are examined for a storm event during year days 315.5 to 317 (November 11-13). The storm produced strong local winds that caused the significant wave height to increase from 0.3m around year day 315.5 to a peak of nearly 3m at year day 316.4, as measured by the FRF 8m bottom pressure gauge array (Figure 3.6). During the storm, wave forcing increased the orbital displacement just above the bottom boundary layer from 0.1m to 1.1m. As the storm tracked out of the region, local wind waves and swell dissipated.

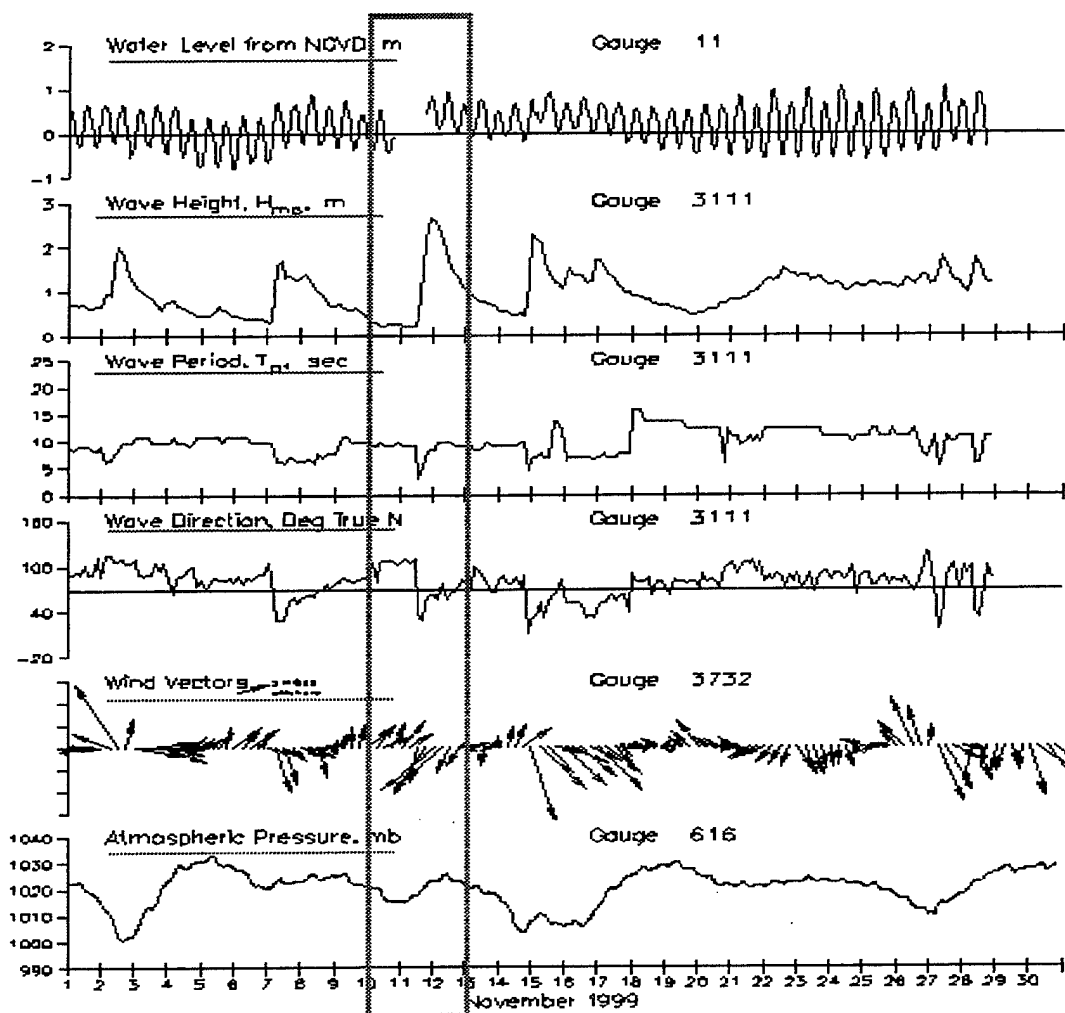


Figure 3.6. FRF Duck, N.C. measured weather and oceanographic data from archived data collection for November 1999. Box indicates the storm event of 10-13 November. (after <http://www.frf.usace.army.mil/>)

The  $u$  and  $v$  velocity components measured by the BCDV were arithmetically averaged over the vertical between 10cm to 30cm above the bed to form 278 second time series at 0.1 year day intervals (2.4 hours). The velocities represent the near-bed velocities just above the turbulent boundary layer, sometimes referred to as  $u_\infty$  and  $v_\infty$ . From the  $u$  and  $v$  time series, the wave oscillatory velocity amplitude,  $U_o$ , peak wave period and mean currents were determined (Figure 3.7).



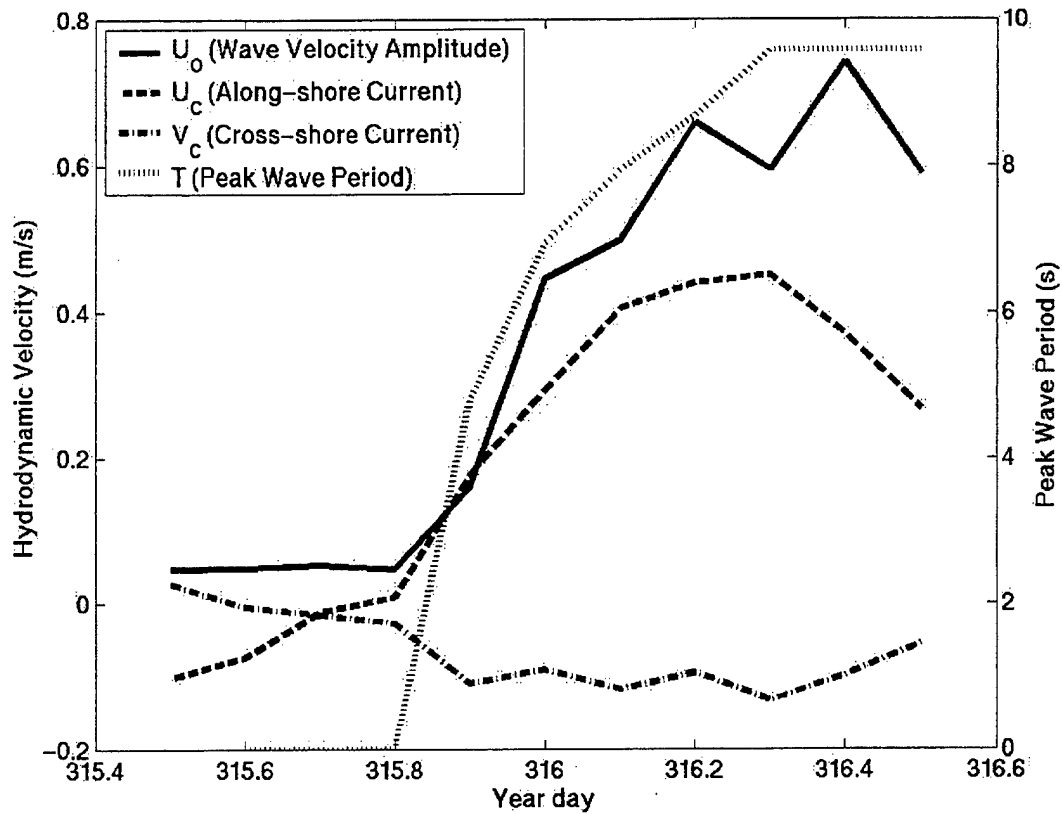


Figure 3.7. Mean currents and oscillatory wave velocity amplitude for year days 315.5 to 316.6 illustrating storm event spin-up of the ocean dynamics.

The wave velocity amplitude is calculated as the equivalent sinusoidal velocity amplitude that gives the same wave variance as measured,

$$U_o = \sqrt{2} \sqrt{\sigma_u^2 + \sigma_v^2} \quad (3.1)$$

where  $\sigma_u^2$  and  $\sigma_v^2$  are the along-shore and cross-shore velocity component variances. The peak wave period of the initially mild waves, composed of local and distant swell was not well defined. By year day 315.9 the storm peak wave period became well defined and increased over the following 24 hours. The majority of the mean current energy was in the along-shore direction as the magnitude increased from 15 cm/s to a

peak of 45 cm/s down-coast. The cross-shore current remained relatively steady at 10 cm/s in the onshore direction.

Bed changes over time obtained from a centerline cross-shore transect of the scanned acoustic altimeter data are shown in Figure (3.8). Initially at year day 315.5, the two-dimensional, cross-shore transect bedform can be described as small-scale vortex ripples overtop a larger scale ripple. The bed became mobile as the dynamic forcing increased. By the peak of the wave and current forcing, the small-scale ripples have been planed-off and the larger scale feature has been flattened.

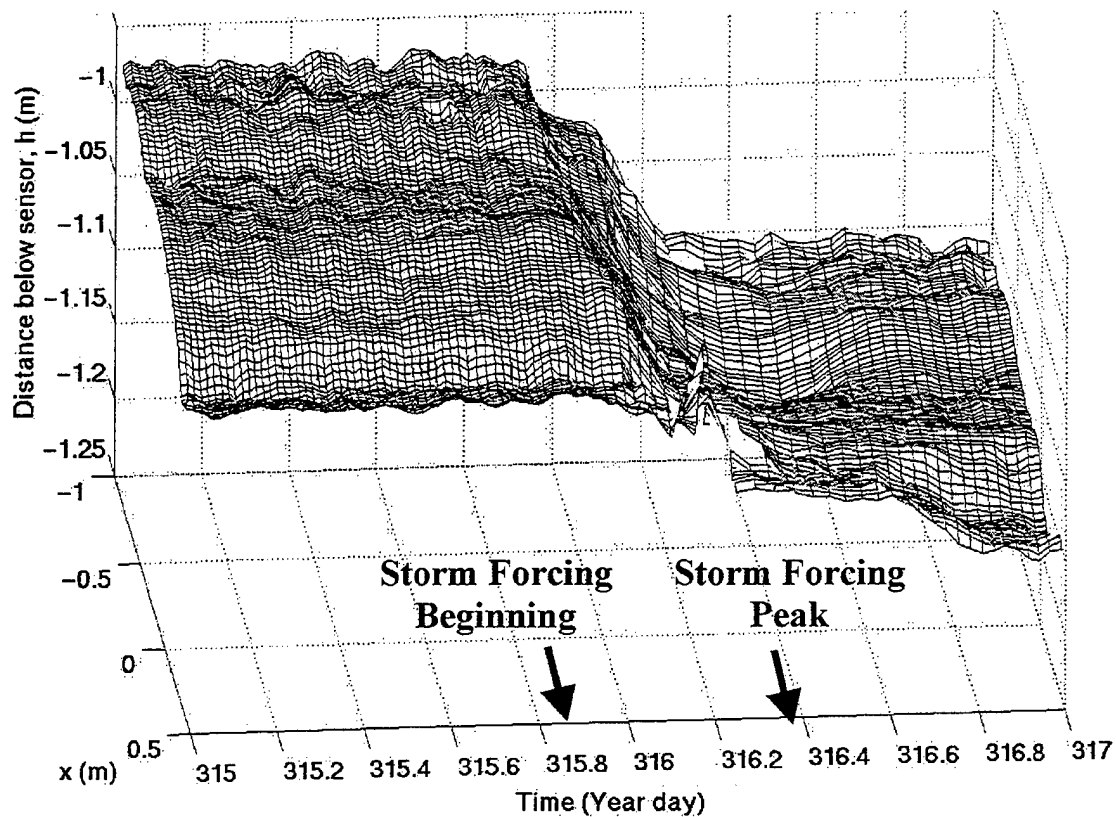


Figure 3.8. Evolution of bedform along centerline, cross-shore transect during storm event. (Positive x direction is towards the beach).

#### IV. DUNE2D MORPHOLOGY OUTPUT ANALYSIS

Sensitivity tests of DUNE2D morphology simulations were first performed to determine model output tendencies given specific monochromatic wave forcing and wave plus current forcing. The model morphology evolution and migration is then compared with field data observed during a storm event of SHOWEX '99. In both studies, a cross-shore transect bedform was chosen from the SHOWEX '99 altimeter data and transformed into a periodic boundary bedform represented in Figure (4.1). All simulations use fine sediment grain diameter equal to 0.1mm, as measured at SHOWEX.

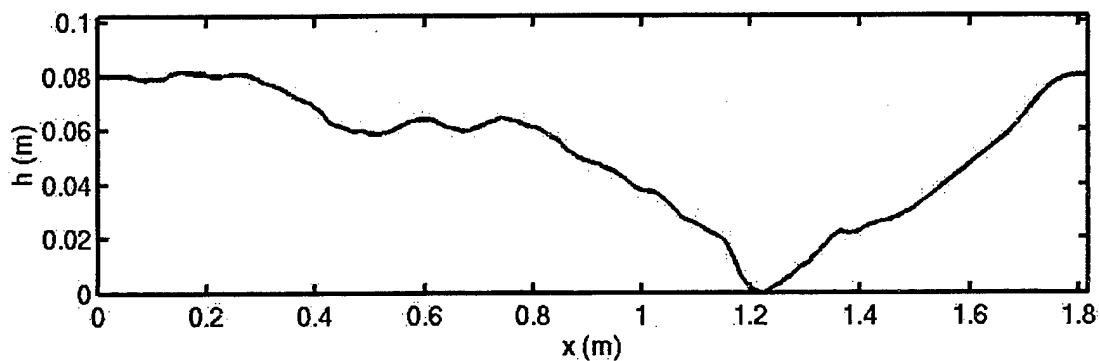


Figure 4.1. Transformed cross-shore transect of bedform from SHOWEX '99 data (year day 315.9) used to initialize DUNE2D simulations. The beach is to the right with the initial oscillatory wave forcing going towards the right (See Appendix (C) for explanation of bedform transformation).

##### A. MODEL SENSITIVITY TESTS

Sensitivity studies of DUNE2D morphology simulations are conducted on the initial bedform (Figure 4.1) using varying initial wave forcing and wave plus current collinear forcing over a short simulation time duration of 20 wave periods to obtain a qualitative feeling for the model performance.

## 1. Wave-only Case Study

Four wave-only forcing tests were made with different monochromatic wave input values as summarized by Table (4.1). Tests 1 and 2 represent the lower wave

Table 4.1. Four test cases in wave-only sensitivity study of morphology simulations.

Wave Input	Test #1	Test #2	Test #3	Test #4
Oscillatory Amplitude, $U_o$ (m/s)	0.35	0.35	0.70	0.70
Period, $T$ (s)	4.8	10.0	4.8	10.0
Orbital Displacement $A$ , (m)	0.23	0.56	0.53	1.1
Mobility Number, $\psi$	76	76	303	303
Field Measured Bedform (Year day)	315.9	315.9	315.9	315.9

energy simulations, with a mobility number,  $\psi$ , equal to 76, indicative of the pre-storm condition. Tests 3 and 4 are the higher wave energy simulations occurring during the storm event, with a  $\psi=303$ .

Bedform changes over twenty wave periods for varying monochromatic oscillatory wave-only forcing is shown in Figures (4.2a-d). In each figure, the output bedforms for the first and twentieth period are displayed. Similar bedform changes resulted for test cases 1 and 2, while test cases 3 and 4 are similar. Vortex ripples are created over top the larger scale bedform in test cases 1 and 2. The amplitude of the vortex ripples is greater for the longer period waves of case 2. The wavelengths are the same for both cases with the average distance between the new ripple peaks is equal to 10cm.

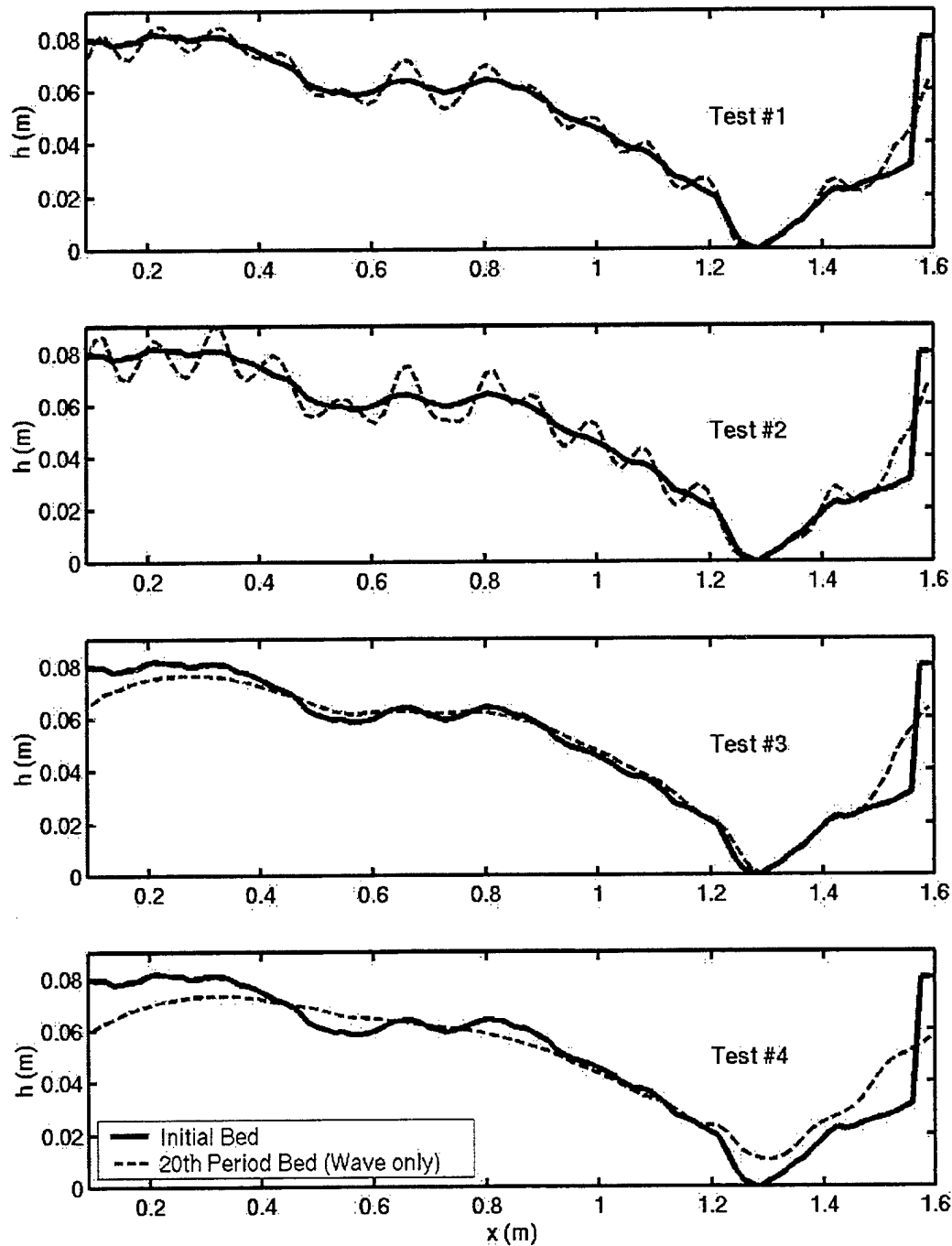


Figure 4.2. DUNE2D bedform morphology for field bedform year day 315.9 with wave-only monochromatic forcing after 20 wave periods. (a) Test#1:  $U_0=0.35$  m/s,  $T=4.79$  s,  $\psi=76$ ; (b) Test#2:  $U_0=0.35$  m/s,  $T=10$  s,  $\psi=76$ ; (c) Test#3:  $U_0=0.70$  m/s,  $T=4.79$  s,  $\psi=303$ ; (d) Test#4:  $U_0=0.70$  m/s,  $T=10$  s,  $\psi=303$ .

For the high mobility number cases 3 and 4, the vortex ripples are planed off, leaving a smoother large-scale bedform. The model tends to quickly change the bed after a short time equal to 5-10 wave periods.

In summary, low energy wave forcing used in tests 1 and 2 results in the creation of vortex ripples on top of the larger scale bedform. The high energy wave forcing used in tests 3 and 4 planes off small-scale ripples on top of the larger scale ripple bedform.

## 2. Wave plus Collinear Current Case Study

The effects of adding a collinear current to the same low amplitude, short period wave forcing and initial field measured bedform (SHOWEX '99 year day 315.9) are examined. Four separate collinear currents (Table 4.2) are considered where the ratio of current to wave velocity amplitude is  $U_c/U_o = 0.5$  (Test 5),  $U_c/U_o = 1.0$  (Test 6),  $U_c/U_o = 2.0$  (Test 7), and a reverse direction current,  $U_c/U_o = -2.0$  (Test 8). Again the model was

Table 4.2. Model hydrodynamic input for wave plus current sensitivity study of morphology simulations.

Hydrodynamic Input	Test #5	Test#6	Test #7	Test #8
$U_o$ (m/s)	0.35	0.35	0.35	0.35
$T$ (s)	4.79	4.79	4.79	4.79
$U_c$ (m/s)	0.175	0.35	0.70	-0.70
$A_r$ (m)	0.23	0.23	0.23	0.23
$\psi$	76	76	76	76
Field Measure Bedform (Year day)	315.9	315.9	315.9	315.9

run for twenty wave periods for each test case with the results shown in Figure (4.3a-d). The results of test case 1 for the wave only forcing are included in the figures for comparison.

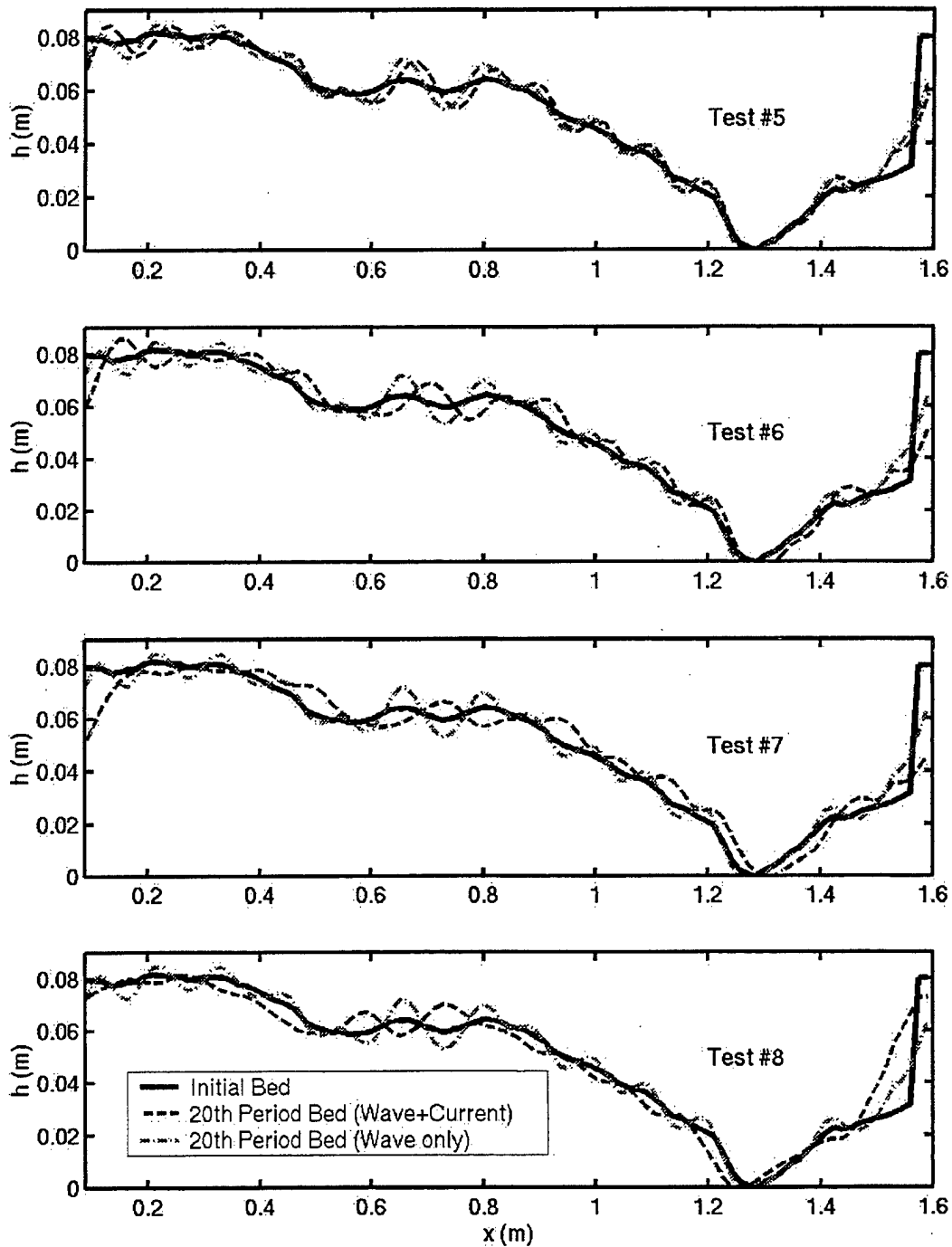


Figure 4.3. DUNE2D bedform morphology given an initial bedform (field year day 315.9) with monochromatic wave ( $U_0=0.35\text{m/s}$ ,  $T=4.8\text{s}$ ,  $\psi=76^\circ$ ) plus current forcing after 20 wave periods. (a) Test#5:  $U_c/U_0=0.5$ ; (b) Test#6  $U_c/U_0=1.0$ ; (c) Test#7:  $U_c/U_0=2.0$ ; (d) Test#8:  $U_c/U_0=-2.0$ .

For  $U_c/U_o = 0.5$  (Figure 4.3a), the current has little effect on the ripple bed. The 20<sup>th</sup> period bedform for test #5 is very similar to the bedform morphology of the wave-only test case, which supports Andersen's (1999) model results for wave plus low current magnitudes ( $U_c/U_o < 0.5$ ) having minor effect on bed morphology. For  $U_c/U_o = 1.0$  (Figure 4.3b), there is a noticeable migration of the bed in the direction of the current. For  $U_c/U_o = 2.0$  (Figure 4.3c), more sediment is removed from the bed and placed into suspension and greater migration of the bed. Finally, reversing the current flow direction 180 degrees, shifts the bed migration to the opposite direction. In summary, a collinear current's effect on the bed is significant at values where the current magnitude is equal to or greater than the wave velocity amplitude,  $U_c/U_o > 1.0$ .

## **B. MODEL COMPARISON WITH SHOWEX '99 OBSERVATIONS**

A DUNE2D morphology simulation of the SHOWEX '99 storm event described in Chapter III was conducted to assess how well the model compares with real-world bedform evolution and migration. In a course of the day, field-measured bedforms experienced low wave energy initially, followed by large wave energy generated by a coastal storm system that resulted in a modified bottom bedform. The bedform evolved from a mega-ripple with superimposed small-scale roughness created by vortex ripples to a flat, smooth bed twenty-four hours later. Refer to Figure (3.7) for the field bedform morphology time series produced by this storm-forcing event.

### **1. Simulation of Storm Event**

The storm event is simulated by two separate model runs representing the initial pre-storm, low wave and current energy, followed by the conditions at the peak wave energy plus current during the storm. The onshore, cross-shore current was low for both



simulations. Most of the current was oriented in the along-shore direction. The orthogonal currents can not be directly included into the simulation since DUNE2D is limited to collinear currents.

An approach to incorporate the effects of the along-shore currents on the bedform is to use an effective wave velocity amplitude that is equivalent to the combined wave and orthogonal current bed shear stress,

$$\tau_{effective} = \tau_b + \tau_c \quad (4.1)$$

where the wave bed shear stress is calculated using Equation (2.14) and the orthogonal current stress is calculated using Soulsby's (1997) equation with a current only drag coefficient.

$$\tau_c = \rho C_D U_c^2 \quad (4.2)$$

$$C_D = \frac{0.4}{1 + \ln\left(\frac{k_n}{30}\right)}$$

From the field measurements, the calculated along-shore, current-only shear stress is 1/3 the wave-only bed stress. Therefore, an effective stress of 133% of the wave-only stress is used to include the effects of the orthogonal current. An effective wave velocity amplitude,  $U_o$ , is obtained from this effective bed stress using Equation (2.14). The results of the modeled, morphology bedform evolution using this effective wave bed shear stress failed because the model generated improper equilibrium ripple lengths and profiles. Therefore, the along-shore current effects on the bedform are assumed not to be

important, which is supported by laboratory results that indicate orthogonal currents do not significantly affect maximum shear stresses under oscillatory flow (Soulsby *et al*, 1993).

Long-time simulations were made to ensure the bed would reach equilibrium, such that accurate ripple geometry measurements could be compared to the field bedforms. The lower energy simulation (Table 4.3., Test #9,  $\psi=16$ ) represents the wave conditions at the beginning of the storm, near year day 315.9. The high-energy waves conditions on year day 316.4 (Table 4.3., Test#10,  $\psi=341$ ) are used to force the initial bedform of year day 315.9 to examine the morphology evolution and migration during the peak of the storm.

Table 4.3. Two test cases in storm event case study of morphology simulations.

Hydrodynamic Input	Test #9 (Low Energy)	Test#10 (High Energy)
Uo (m/s)	0.16	0.74
T (s)	4.8	9.6
Uc (m/s)	0.11	0.10
$\psi$	16	341
A <sub>s</sub> (m)	0.12	1.13
Bedform (Year day)	315.9	315.9
Total Simulation Time (s)	9580	9580

The simulated bedform morphology time series are shown in Figures (4.4) and (4.5a) for the low hydrodynamic energy with the field bedform morphology evolution following the same forcing given in Figure (4.5b) for comparison. The modeled morphology for the high energy simulation (test #10) is illustrated in Figures (4.6) and (4.7a), with the field bedform results in Figure (4.7b) for comparison.

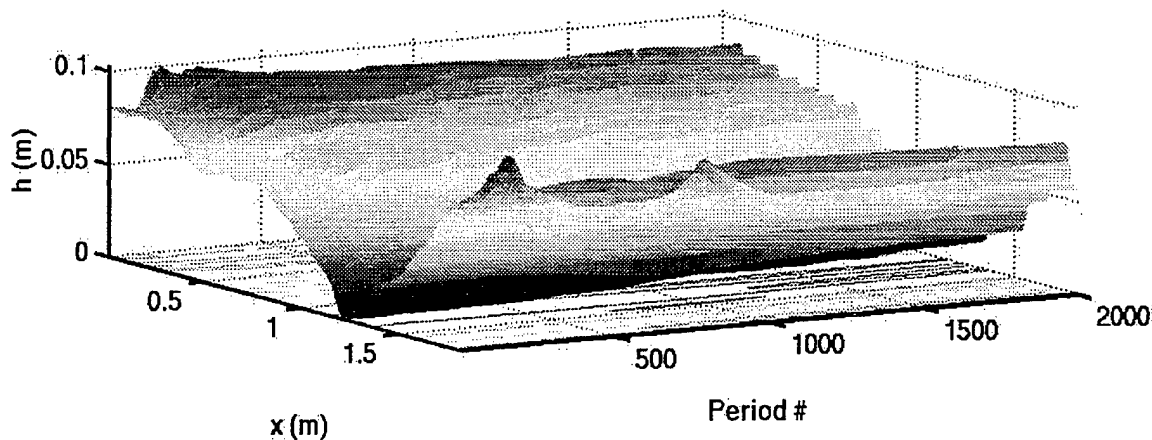


Figure 4.4. Test#9: DUNE2D morphology time series given an initial bedform (year day 315.9) with low wave energy ( $U_o=0.16$ ,  $T=4.8$ ,  $U_c=-.11$ ,  $\psi=16$ ,  $A=0.12m$ ).

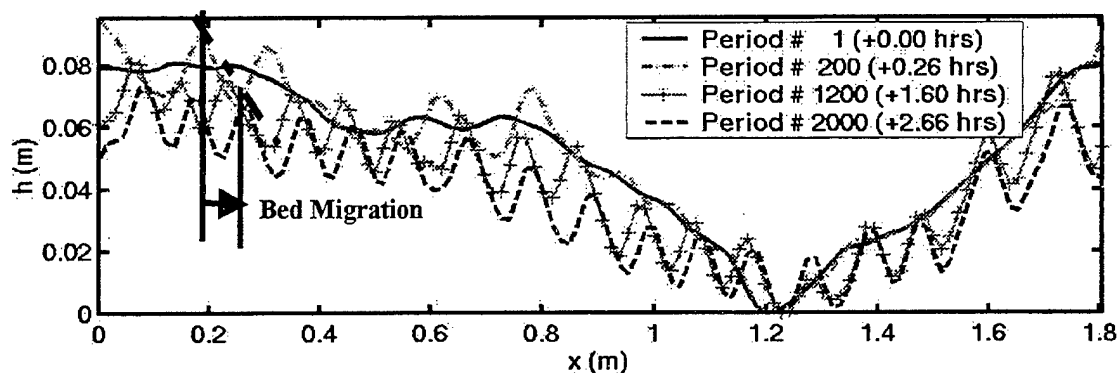


Figure 4.5a. Test #9: DUNE2D morphology bedform snapshots over simulation time resulting in a vortex ripple field at equilibrium state (ripple geometry:  $\lambda_{Avg}=0.11m$ ,  $\eta_{Avg}$  (height) =  $0.02m$ ,  $\eta_{Avg} / \lambda_{Avg}$  (slope) =  $0.18$ ,  $\lambda_{Avg}/A = 0.92$ ). Migration:  $4.2cm/hr$  onshore.

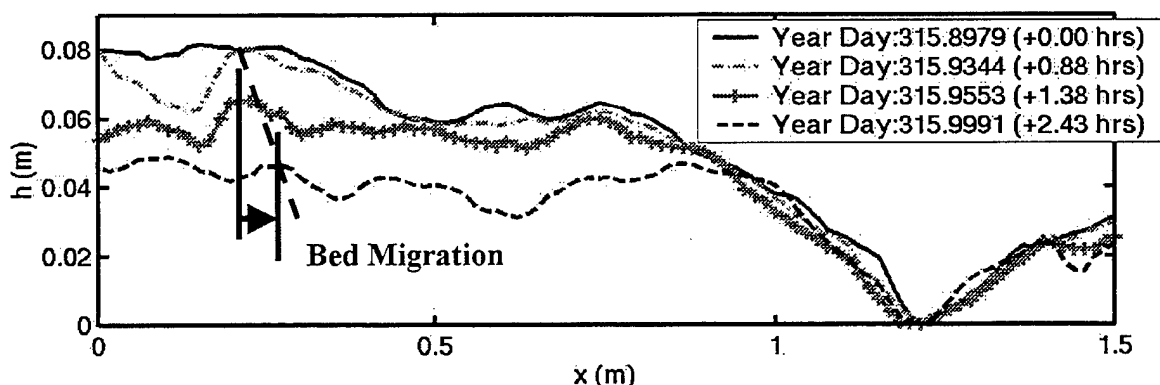


Figure 4.5b. SHOWEX '99 Bedform morphology time series snap shots taken from year day 315.9 to 2.4 hours later. (superimposed vortex ripple geometry:  $\lambda_{Avg}=0.2m$ ,  $\eta_{Avg} = 0.008m$ ,  $\eta_{Avg} / \lambda_{Avg} = 0.04$ ) Migration:  $4.5cm/hr$  onshore

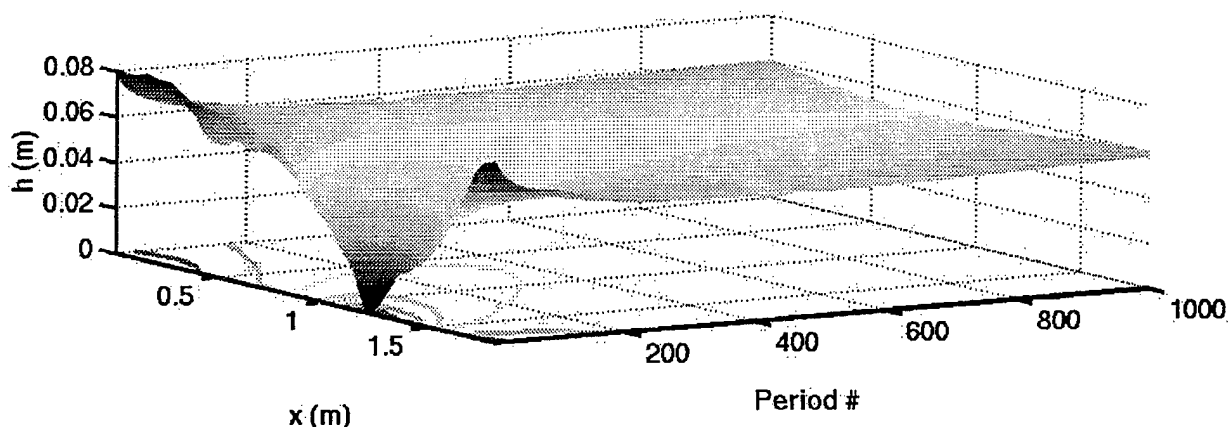


Figure 4.6. Test#10: DUNE2D morphology time series given an initial bedform (year day 315.9) with high wave energy ( $U_0=0.74$ ,  $T=9.6$ ,  $U_c=-0.1$ ,  $\psi=341$ ,  $A=1.1\text{m}$ ).

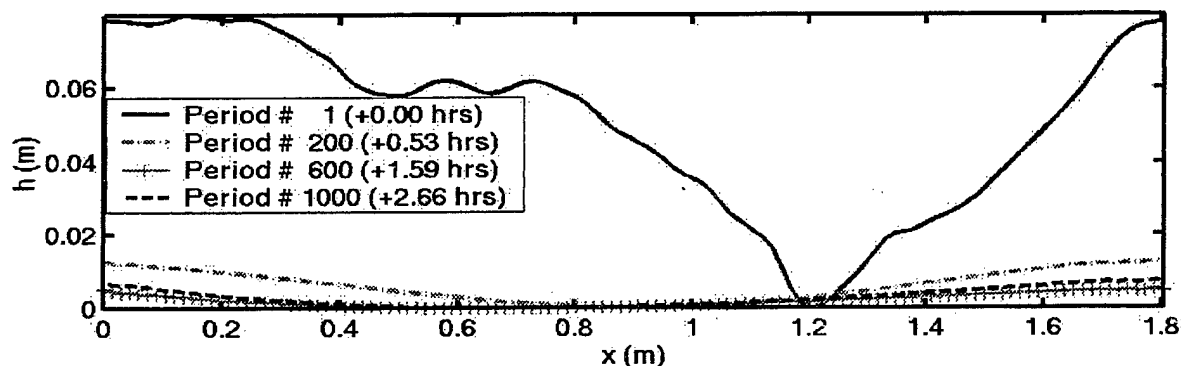


Figure 4.7a. Test #10: DUNE2D Model morphology bedform snapshots over simulation time resulting in a flat mega-ripple equilibrium state (ripple geometry:  $\lambda_{\text{Average}}=1.8\text{m}$ ,  $\eta = 0.008\text{m}$ ,  $\eta/\lambda = 0.005$ ,  $\lambda_{\text{Average}}/A = 1.5$ ).

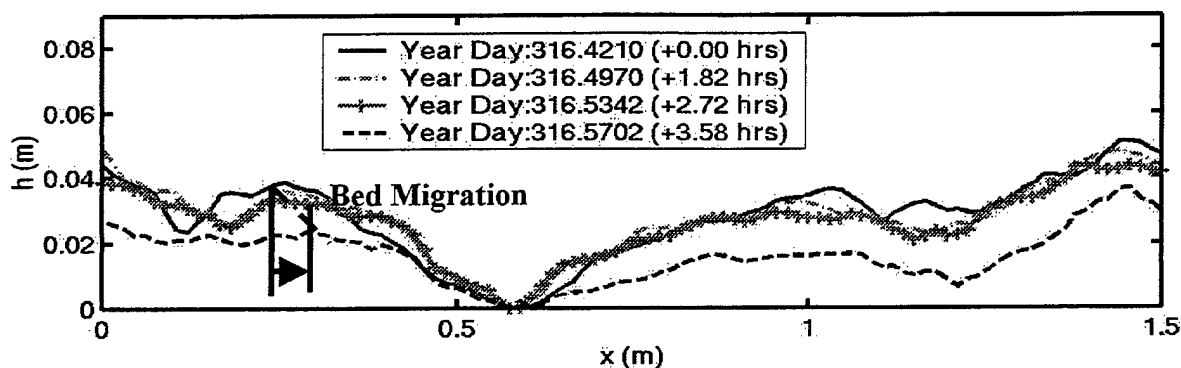


Figure 4.7b. SHOWEX '99 Bedform morphology time series snap shots taken from year day 316.4 (bedform during peak wave forcing) to 3.6 hours later. (Ripple geometry:  $\lambda_{\text{Average}}=1.5\text{m}$ ,  $\eta = 0.02\text{m}$ ,  $\eta/\lambda = 0.02$ ). Migration:  $2.2\text{ cm/hr}$  on-shore.

## 2. Discussion of Storm Event Simulation

The low energy simulation (test #9) reached equilibrium after about 2000 wave periods (+2.6hrs). The bedform is characterized by small-scaled vortex ripples over top a larger scale ripple, much like the field bedform (Figure 4.5b). The average wavelength of the vortex ripples at equilibrium state is 0.11 m, with an average height of 0.02m. A ratio of average ripple wavelength to orbital displacement is approximately equal to one. This compares qualitatively well with the observed bedform during the low wave energy state and with Neilsen's (1981) equation (3.4.3) for  $\sqrt{2}(\lambda/A)$ , given  $\psi < 200$ . The slope of the measured vortex ripples superimposed over the larger scale ripple (Figure 4.5b) is 0.04 compared with the modeled ripples slope of 0.18. Some of the difference is due to the field instrument's 4cm spatial roll-off in the horizontal that flattens off the top of the small-scale ripples of the bed. However, since the observed forcing had a finite spectral width and directional spread, the SHOWEX forcing does not closely match the single frequency unidirectional model forcing. The migration of the modeled vortex ripple is 4.2 cm/hr onshore, while the field bedform is similar at 4.5 cm/hr onshore. A summary of the results is given in Table (4.4).

Table 4.4. Storm event ripple geometry comparison (DUNE2D vs. SHOWEX)

Ripple Geometry Output	Low Energy Forcing		High Energy Forcing	
	DUNE2D Test #9	SHOWEX (YR 315.9)	DUNE2D Test #10	SHOWEX (YR 316.57)
$\lambda_{Avg}$ (m)	0.11	0.20	1.8	1.5
$\eta_{Avg}$ (m)	0.02	0.008	0.008	0.02
Slope ( $\eta_{Avg}/\lambda_{Avg}$ )	0.18	0.04	0.004	0.01
$\lambda_{Avg}/A$ (m)	0.92	1.7	1.5	1.4
Migration (cm/hr)	4.2	4.5	Unresolved	2.2

The high-energy simulation (test #10) reaches equilibrium in about 1000 wave periods (+2.6 hours), faster than the field bedform (+3.6 hours). The average wavelength of the flat, large-scale ripple is 1.8 m, with a height of 0.008 m. The ratio of ripple wavelength to orbital displacement is around 1.5. The simulated large-scale, flat ripple has a similar dip in the middle of the bed with higher peaks towards the ends of the boundaries as the field bedform (Figure 4.7b). The modeled migration rate is unresolved, while the measured bed, under the high energy forcing, migrates at 2.2 cm/hr onshore.

A question arises with the ripple geometry for the high energy simulation (Test #10) as to whether its equilibrium bedform is influenced by the domain size of the grid, as the computed equilibrium ripple wavelength,  $\lambda_{Avg}$ , appears to be equal to the horizontal domain of the model run. (Figure 4.7a) To examine the question, four separate model runs were performed where the length of the domain of the initial bedform was varied, as summarized in Table (4.5) and Figure (4.8a-d).

Table 4.5. Grid test cases to verify boundary effects on morphology simulations.

Hydrodynamic Input	Test #11	Test#12	Test#13	Test #14
$U_o$ (m/s), $T$ (s), $\psi$	0.69 , 9.6 , 292			
$A_o$ (m)	1.05			
Initial Bedform (Year day)	315.9			
DUNE2D Bedform Horizontal Distance Increase from Original Bed	30%	50%	100%	300%
Total Simulation Time (s )	9580			

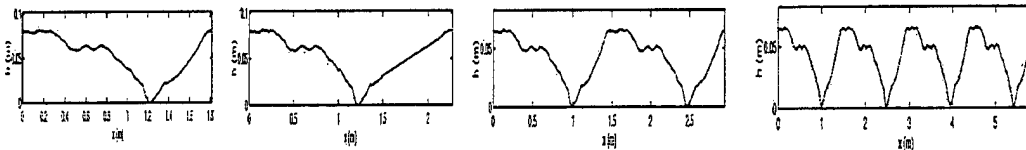


Figure 4.8. DUNE2D initial bedform for (a)Test #11,(b) Test #12, (c) Test #13 (d) Test #14.

The high energy model simulations, with similar forcing as test #10, produce different equilibrium ripple wavelengths than measured (Figure 4.9a-d). The model

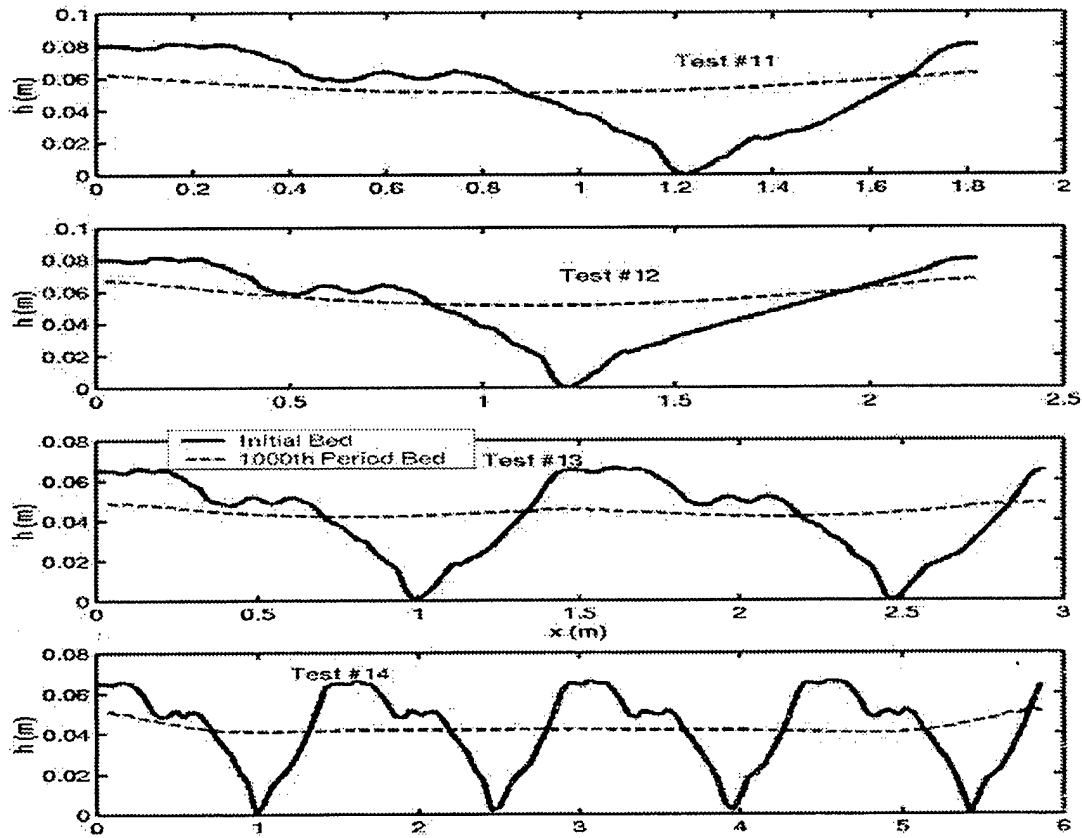


Figure 4.9. DUNE2D morphology simulations illustrating bedform evolution at equilibrium (+2.6hrs) for (a) Test #11 ( $\lambda_{Avg}=1.8m$ ), (b) Test #12 ( $\lambda_{Avg}=2.2m$ ), (c) Test #13 ( $\lambda_{Avg}=1.5m$ ). (d) Test #14 (unresolved  $\lambda_{Avg}$ )

output for the 30% and 50% bedform enlargement produce single mode bedforms with wavelengths equal to the total horizontal domain, 1.8m and 2.2m, respectively. A doubled domain with two bedforms produces two flatten ripples with an average wavelength equal to 1.5m, about half of the total horizontal domain. Test #4 has an unresolved equilibrium wavelength due to the large perturbation at the domain ends. The four tests show the equilibrium wavelength of the large-scale ripple that evolves under

high energy forcing (forcing capable of removing vortex ripples) is affected by the horizontal domain of the initial bedform. Therefore, the high energy results can be only qualitatively compared with the field bedform. The modeled equilibrium bedform show similar removal of vortex ripples and a flattened, large-scale ripple for high energy forcing as the field measurements.

### **C. WAVE SIMULATION OF FIELD STORM EVENT**

DUNE2D is limited to monochromatic wave forcing. However, the field data show narrow-banded wave forcing with some groupiness present. To simulate the groupiness of the field measured waves, a sequence of monochromatic wave model runs was performed. Each successive model run was represented by the equivalent wave velocity amplitude and period of the measured waves. The duration of each run was equal to the measured duration of the section of real wave condition, so that a piecewise narrow band forcing time series could be constructed. Additionally, each model run was initiated by the previous final morphology bedform output and flow solutions.

However, the method failed when trying to initialize the successive runs with the previous bedform output and flow solutions. For the case of a moveable bed as used in these simulations, the initial bedform is normalized by a scaling parameter,  $D$ , which is based on the monochromatic forcing input ( $U_0$  and  $T$ ). The model generates a grid from this initial, normalized bedform. When the successive model runs are initiated with the previous output bedform and flow solutions, the model is unable to resolve the new flow solutions due to different scaling values used to generate dissimilar grids between the two model runs. Further work is required to incorporate the amplitude changes associated with groupiness waves that are representative of the real world.



## V. CONCLUSION

The migration and evolution of small-scale bedforms was simulated using DUNE2D based on field hydrodynamic forcing of the bottom boundary layer. The model simulates flow, sediment transport, and morphology in the bottom boundary layer to enable bedform comparisons with the field data. The initial cross-shore bedform used in the model closely matched the measured SHOWEX acoustic altimeter data. However, it is required to manipulate the measured bedform to conform to the cyclic boundary requirement. At low energy forcing, the model generated vortex ripples. The equilibrium wavelengths of the rippled bedforms were near the orbital diameter for the oscillatory wave forcing. SHOWEX bedform changes under low wave plus collinear current conditions resulted in minor changes of the vortex ripple fields. Bedform migration rates of the model were similar to the field migration rates.

DUNE2D simulations of high energy forcing over a ripple bed resulted in greater change in the bed over a shorter duration of time compared with the lower energy forcing simulation. Like the field data, the modeled data under strong forcing removed smaller scale vortex ripples and redistributed the sediment into a larger scale ripple with a large portion of sediments in suspension above the bed. Final equilibrium bedforms consisted of larger scale, flattened ripples with wavelengths reaching beyond orbital excursion values. However, the horizontal domain of the initial bedform and the number of initial low-mode ripples was found to be somewhat influenced by the equilibrium ripple wavelength of the large-scale ripple that evolved under high energy forcing.

In nature, sediment sizes and distribution varies spatially and temporally. The model simulations are limited to a single sediment grain diameter designation, which in turn affects the Shield parameter calculations. Ultimately, the Shield's parameter calculations relate to sediment transport and bedform morphology accuracy.

The oceanic wave forcing is not monochromatic and unidirectional, so detailed comparisons with DUNE2D model are not possible. However, the modeled bedform data was compared qualitatively with changes in the measured bedforms (Table 4.4). Differences can be ascribed to model input limitations, which include simple sinusoidal wave forcing, collinear current directionality, periodic bedform boundaries, and single sediment grain diameter selection. Efforts focused on generalizing the wave forcing to simulate actual field conditions and initial bed configuration. Simulation of the storm event through sinusoidal flow over bedforms restricted actual simulation of real waves. The higher energy SHOWEX velocity fields were characterized by groupy waves. Wave simulation could not duplicate the groupiness observed in the field. The inability to vary current direction within the model reduced proper sediment transport. During the storm event, strong along-shore current existed. Simulation of collinear currents demonstrated substantial transport when currents are greater than the velocity amplitude,  $U_c/U_o > 1.0$ . Despite the inability to establish arbitrary wave forcing and directional currents, the model bedform tendencies based on the simple forcing provided good qualitative agreement with field bedforms. Continued work on the capability of the model to incorporate real world wave and current forcing is encouraged. The model provides a good basis for which to better understand the probable bed migration and evolution over time given near monochromatic wave forcing in the nearshore.

## APPENDIX A. DUNE2D MODEL SOLUTION

This appendix provides detailed discussion of DUNE2D model solutions. The following sections are divided between model input and output descriptions.

### A. MODEL INPUT

Hydrodynamic forcing, geophysical properties of the sediment, numerical schemes, grid definitions, boundary conditions, transport methods, and morphology setup are discussed below.

#### 1. Hydrodynamic and Geophysical Input

The model is forced by monochromatic sinusoidal wave motion. Wave motion is described by the amplitude of the oscillatory wave velocity,  $U_o$ , and period,  $T$ . Implementation of a current in the same direction as the wave is an option. The scaling depth,  $D$ , is applied to most input terms to provide non-dimensionality where

$$D = 2\pi\alpha = U_o T \quad (\text{A.1})$$

The model is based on turbulent boundary flow. The flow is characterized by the Reynolds number computation as described below:

$$R_e = \frac{U_o D}{\nu}; \quad \nu = \text{kinematic viscosity} \quad (\text{A.2})$$

Sediment description is limited to a homogeneous bottom type, described by the medium grain diameter,  $d_{50}$ . The grain diameter is incorporated into the model through the roughness of the bottom,  $k_n$  (Equation 2.10). (Fredsoe and Deigaard, 1992) Porosity of the sediment is set at 0.4. The ratio of sediment density,  $\rho_s$ , to water density,  $\rho$ , is constant at 2.65, based on in-situ sand samples.

Model simulation time is based on total number of wave periods. Time steps,  $\Delta t$ , are a function of the number of iterations for each wave period. Both time functions are described by the DUNE2D model input variable WAVE.

Table A.1. Hydrodynamic and geophysical input.

DUNE2D Variable	Physical Parameter
ROUG	Non-dimensional Nikuradse constant, $k_n/D$
ANGU	Non-dimensional depth, $D/a$
WAVE	Total number of wave periods & iterations per period
TURB	Reynolds number, $R_e$

## 2. Numerics and Scheme Setup

A finite volume numerical method is used to discretize the general flow equations in section (2.3). The flow is assumed to be incompressible. The pressure term in the Reynolds-averaged Navier-Stokes (RNS) equations is calculated using the PISO algorithm (Patankar, 1980). The PISO algorithm is an iterative process used to determine the pressure values at each grid point. The user provides the number of times the PISO algorithm is implemented. For flows that are difficult to converge, a higher number of iterations are required. Andersen emphasizes the difficulty of solving the pressure term within the RNS equations.

Zijlema's (1996) ISNAS scheme, a high order spatial discretization method, is used to remove numerical diffusion errors. Implicit time discretization methods are utilized, except for the advection terms where semi-implicit techniques are implemented.

Table A.2. Numerical Input.

DUNE2D Variable	Physical Parameter
SCHM	Discretization using ISNAS scheme
PISO	PISO algorithm parameter
TURB	$\kappa$ - $\omega$ turbulent closure model

### 3. Grid Input

For morphology simulations, the grid is generated using a transfinite interpolation technique. The transfinite interpolation technique produces finer resolution at the bed, while vertically stretching the grid points out as the distance from the bed increases. A specific constant, GMET, is used to define the degree of stretching. Large GMET values correspond to increased stretching. Additionally, the total number of vertical coordinate points,  $M$ , is a function of the transfinite interpolation method.

The user can specify bedform through an ASCII file or have DUNE2D generate a bottom using several predefined bedform shapes. For user-specified bedforms, the ASCII file contains information about the number of horizontal,  $N$ , and vertical,  $M$ , grid points. Also, the file contains the bedform grid values normalized by the scaling term,  $D$ . An example of a grid file, *test.grd*, is given in Appendix (B).

The resolution of the grid spacing is set by the bed roughness, which is a function of the bedform profile, Nikuradse constant, sediment grain diameter and wave forcing input. From Fredsoe and Deigaard, the relationship used to determine the resolution parameter,  $RESO$ , requires the calculation of the maximum frictional velocity,  $u'_*$ ,

$$u^* = 0.1\sqrt{2}U_o\left(\frac{k_n}{a}\right)^{0.125}$$

$$\text{RESO} = \text{integer}\left(\frac{2.5}{0.4}d_{50}\frac{u^*}{\nu}\right)$$
(A.3)

RESO is used in the grid generating procedure. Large RESO values are indicative of the higher grid resolution.

Table A.3. Grid Input.

DUNE2D Variable	Physical Parameter
GRID	N: horizontal total grid pts; M: vertical grid pts
RESO	Grid Resolution parameter
GMET	TFI grid generator stretching parameter

An example of a generated grid using the transfinite interpolation technique over a user-defined bedform is shown in Figure (A.1).

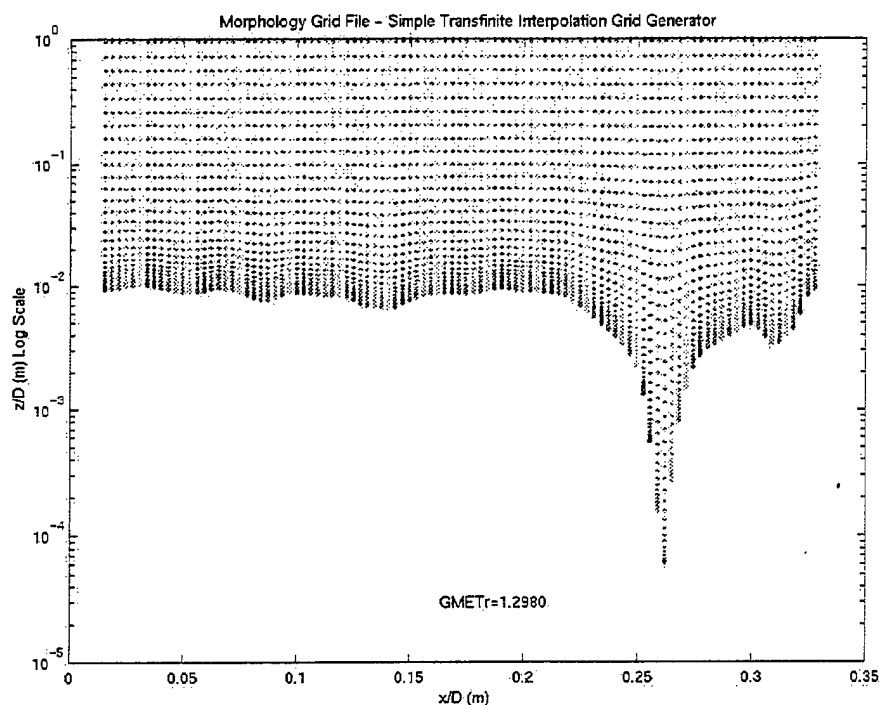


Figure A.1. DUNE2D grid using the transfinite interpolation method.

#### 4. Grid Sensitivity Study

A grid sensitivity test of the flow performed by Andersen (1999) is summarized in Table (A.6). Four parameters were tested:  $y^+$ ,  $M$ ,  $\Delta x_{\text{crest}}/a$ , and  $D$ . The first term,  $y^+$ , is the distance from the bottom boundary to the first grid point. Flow around the crest of the ripples was found to be sensitive to the bed slope. A stretched grid was applied to enhance the number of points in that region. Therefore, the value  $\Delta x_{\text{crest}}$ , the horizontal spacing between grid points around the crest, was tested.  $D$  is the normalized depth of the flow. The tests provide guidance on model performance, in particular on flow convergence and numerical stability.

Table A.4. Grid Sensitivity of the Flow Test Results.

$y^+$	$\leq 0.40$
$N \times M$	40X30
$\Delta x_{\text{crest}}/a$	$\leq 0.012$
$D$	$\geq 5.0 \cdot a$

Andersen also performed a grid sensitivity test for the suspended load. By varying the total vertical grid points between 40, 60, and 100, little was achieved in grid convergence of the suspended concentration above the bed.

#### 5. Model Boundary Conditions

The lateral boundary conditions are periodic. Bottom boundary conditions are:

$$\frac{\partial(\quad)}{\partial z} = 0 \quad u, w = 0 \text{ at the } z = D$$

The no-slip condition creates a viscous sub-layer. The top boundary is described by a symmetric boundary condition.

## 6. Sediment Transport Related Setup

Bedload and bed concentration formula are based on Engelund and Fredsoe formulation, which is described in Chapter II. Angle of repose of the sediment is constant at 0.65. Critical Shields parameter is 0.05 for all model runs.

The sediment fall velocity is calculated using Fredsoe and Deigaard's empirical relationship for sand using an iterative process of Equation (2.17).

Suspended load along the lateral boundaries is treated as a true cyclic boundary. Additionally, wall boundary techniques are used to separate the suspended load from bedload. The bed concentration is assumed to be based on normal diffusion.

Table A.5. Sediment Transport Input.

DUNE2D Variable	Physical Parameter
BEDL, BEDC	Bedload and Bed concentration formula using Engelund-Fredsoe formula
FALL	Non-dimensional settling velocity of the sediment
SSLO	Wall boundary option for suspended load
SMIX	Normal diffusion of bed concentration
SSCY	True-cyclic suspended load

## 7. Morphology Setup

Once the morphology mode is turned on, only a few additional DUNE2D variables are required. The QUICK scheme with top smoothing is applied to the solution



of the continuity equation in the morphology section below. This is third order accurate. (Andersen, 1999). The smoothing is based on a running average.

Table A.6. Morphology Input.

DUNE2D Variable	Physical Parameter
MSCH	Leonard (1979)'s Quick Scheme for continuity equation
QSMO	Smoothing is iterated 4 times over bed and at ripple crests

## B. MODEL OUTPUT

Figure (A.2) summarizes output parameters from each of the three modules.

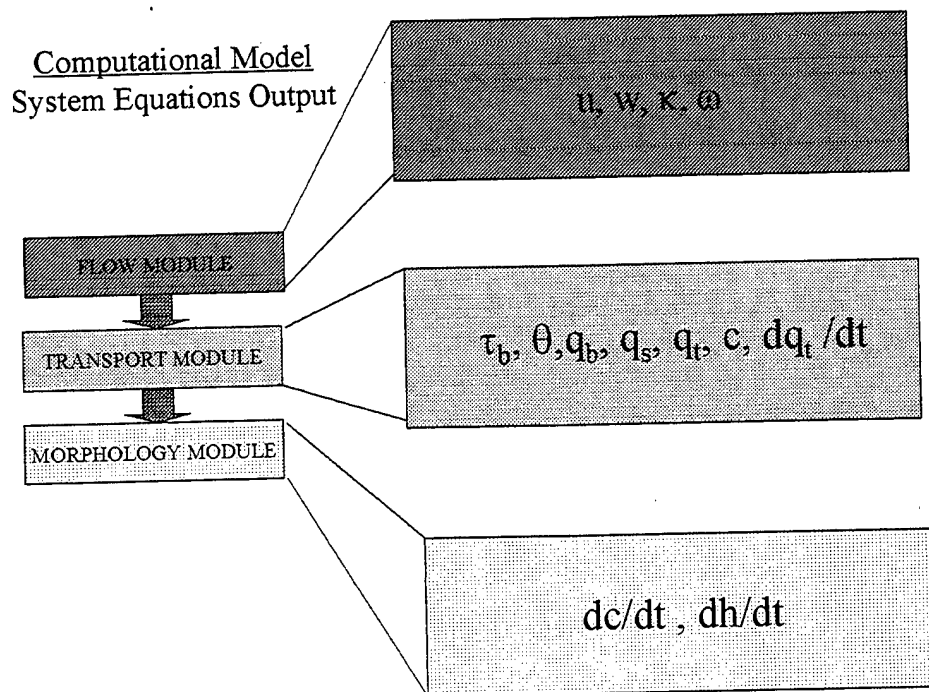


Figure A.2. DUNE2D Module Output Diagram.

The morphology mode simulation produces time-averaged quantities over a single wave period. Table (A.7) summarizes the different output variables that are saved to

ASCII files by DUNE2D. Most of the output is non-dimensional. Transformation of these quantities into meaningful dimensional output will be discussed in Appendix (C).

Table A.7. Morphology Mode Output. (Period Average Mean).

Output	Physical Parameter
$\langle \tau_b \rangle_t$	Bed shear, time averaged over one wave period
$\langle \theta \rangle_t$	Shield parameter, time averaged over one wave period
$\langle q_b \rangle_t$	Bedload flux, time averaged over one wave period
$\langle q_s \rangle_t$	Suspended load flux, time averaged over one wave period
$\langle q_t \rangle_t$	Total load flux, time averaged over one wave period
$\langle \phi_t \rangle_t$	Non-dimensional total load flux, time averaged over one wave period
$\langle c \rangle_t$	Bed concentration, time averaged over one wave period
$\langle U \rangle_t$	Horizontal velocity, time averaged over one wave period
$\langle W \rangle_t$	Vertical velocity, time averaged over one wave period
$\langle Dh/dt \rangle_t$	Change in bed form w/ time, time averaged over one wave period
$\langle h \rangle_t$	Bed form height, time averaged over one wave period

## APPENDIX B. DUNE2D MODEL APPLICATION

This appendix provides further information on the application of DUNE2D code. The first section describes general DUNE2D Fortran file information, as well as model initiation. The following section emphasizes input file examples.

### A. FORTRAN CODE FILES

DUNE2D is a modular Fortran 77 code program consisting of (16) \*.f programs, (9) \*.i programs, and a *makefile*. The code is divided into logical modules designed around the model input, flow calculations, bedload transport computations, morphology solutions, and output. The *makefile* is designed to compile all the programs into a single executable program called *dune*. A list of programs is given by Table (B.1).

In the Unix environment, typing *dune* followed by a string four-letter project name, e. g. "*test*", will execute the simulation application. Other files are required to run DUNE2D. These will be discussed in the next section.

Table B.1. Fortran DUNE2D Files. {Program areas: a)I/O: input/output b)F: flow c)S: sediment transport d)M: morphology e)G/B: grid/boundary}

b.f: G/B	cmd.f: I/O	dune2d.f: main	ff: F
g.f: G/B	i.f: I/O	io.f: I/O	isolines.f: G/B
k.f: F	ko.f: F	m.f: F	profile.f: F
p.f: F	r.f: F	ripple.f: G/B	susp.f: S
s.f: S	t.f: F	wave.f: F	wavemorph.f: M

## **B. MODEL INITIATION FILES**

Once an error-free compiled version of *dune* exists, simulation can begin with the proper input files in place. The files have \*.inp, \*.grd, and \*.fmt file extension, which represent input, grid, and format ASCII files. The three files must have the same four letter project name that is typed after *dune*, e. g. *test.inp*, *test.grd*, and *test.fmt*. Additionally, special input files, *Special.inp* and *Equations.inp*, must be included in the simulation folder. These two files are used to initiate DUNE2D simulation

### **1. Input File**

The input file, *test.inp*, describes the necessary input variables used to describe model calculation, initiation, hydrodynamic forcing, total time of integration, and other requirements used in flow, bedload transport, and morphology modules described in Chapter II. Appendix (A) provides greater detail on the specific requirements of the input file. An example is provided at the end of this section.

### **2. Grid File**

The grid file, *test.grd* or *test.xyb*, is a two-column, ASCII file that describes the initial bedform grid point locations. User-defined grids are described by \*.xyb files that are the same format as \*.grd files. An example has been included.

### **3. Format File**

Finally, the format file is used to describe the boundary conditions of the model. Since all model runs for this thesis and the work by Andersen (1999) only use a single block, the format file was not required in the model simulation. For more information on the model boundary conditions refer to Appendix (A).

Example of input file: test.inp

# General commands: test.inp 03-Nov-2000

READ, 0, 0.0  
COUT, 0, 0.0  
GOUT, 0, 0.0  
SCRE, 10, 0.0  
PISO, 3, 0.0

# Commands for the solver:

ZTOP, 1, 0.0  
TURB, 4, 5.87e+05  
INIT, 2, 0.0  
SCHM, 4, 1.0000  
SKEW, 1, 0.0

# Setup of the grid:

COOR, 1, 0.0  
GRID, 100, 40.0000  
GMET, 4, 1.2980  
RESO, 13, 0.0

# Bed load transport:

BEDL, 1, 0.0  
ROUG, 0, 0.0001  
TTOP, 1, 0.0863  
SPHI, 0, 0.5770

# Suspended transport:

SUSP, 1, 0.0  
SSCY, 3, 0.0  
SSLO, 1, 0.0  
BEDC, 0, 0.0  
SMIX, 0, 0.0  
FALL, 2, 0.0168

# Setup of the wave:

DYNA, 1, 0.0  
ANGU, 0, 6.2832  
WAVE, 20, 1000.0000  
WEND, 0, 1.00e-24  
MEAN, 1, 0.0

# Morphology Module:

MORP, 1, 0.0  
MOUT, 150, 0.0  
MOIT, 5, 0.0  
MSCH, 8, 0.0  
QSMO, 4, 4.0000  
MRLX, 0, 1.0000

# User defined variables:

PROB, 0, 0.0

Partial Example of test.xyb

120	40
0.00000000	-0.00265241
0.00261905	-0.00285512
0.00523809	-0.00189552
0.00785714	-0.00112030
0.01047619	-0.00080800
0.01309524	-0.00013576
0.01571429	0.00004675
0.01833333	0.00102395
0.02095238	0.00214214
0.02357143	0.00334799
0.02619048	0.00452660
0.02880952	0.00567079
0.03142857	0.00685681
0.03404762	0.00804007
0.03666667	0.00920828
0.03928571	0.01034211
0.04190476	0.01155320
0.04452381	0.01285784
0.04714286	0.01420774
0.04976190	0.01547332
0.05238095	0.01666995
0.05500000	0.01779334
0.05761905	0.01893293
0.06023810	0.02016495
0.06285714	0.02150976
0.06547619	0.02288504
0.06809524	0.02416856
0.07071429	0.02539719
0.07333333	0.02664316
0.07595238	0.02788491
0.07857143	0.02913498
0.08119048	0.03033831
0.08380952	0.03156390
0.08642857	0.03283032
0.08904762	0.03408979
0.09166667	0.03537232
0.09428571	0.03657105
0.09690476	0.03779511
0.09952381	0.03902313
0.10214290	0.04032772
0.10476190	0.04169318
0.10738100	0.

Program break. Note the first line is the total number of horizontal and vertical points.

#### 4. Summary

Summaries of the required files for simulation are given by Table (B.2). These files should all be placed in the same Unix folder.

Table B.2. Files necessary for simulation. (\*user option, not required)

DUNE2D file	Description
<i>dune</i>	Fortran 77 compiled executable file
<i>"test".inp</i>	Input variables
<i>Special.inp</i> <i>Equations.inp</i>	Special input files (no user input required)
<i>"test".grd</i>	Initial bedform bottom grid *

A schematic flow chart of the input/output procedure using the required input files is shown in Figure (B.1).

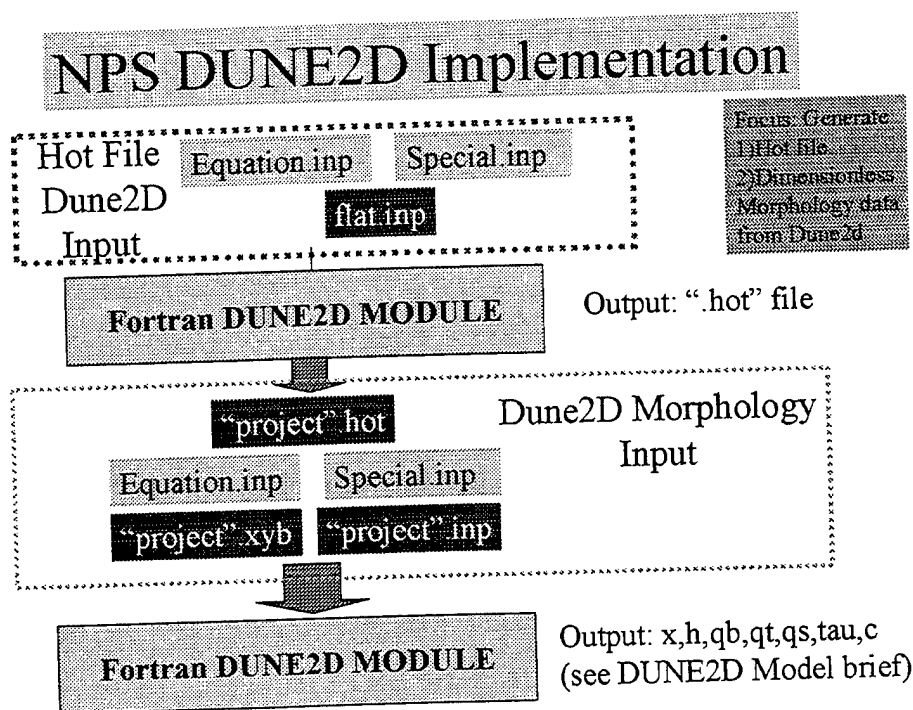


Figure B.1. DUNE2D input/output flow diagram.

THIS PAGE INTENTIONALLY LEFT BLANK



## APPENDIX C. DUNE2D INPUT/OUTPUT TRANSFORMATION

This appendix provides specific input and output procedures used to implement DUNE2D code. An overview of the process by which data is entered into the DUNE2D Fortran format input files as well as transformation of the output files into meaningful, dimensional, as well as, graphical results is shown in Figure (C.1).

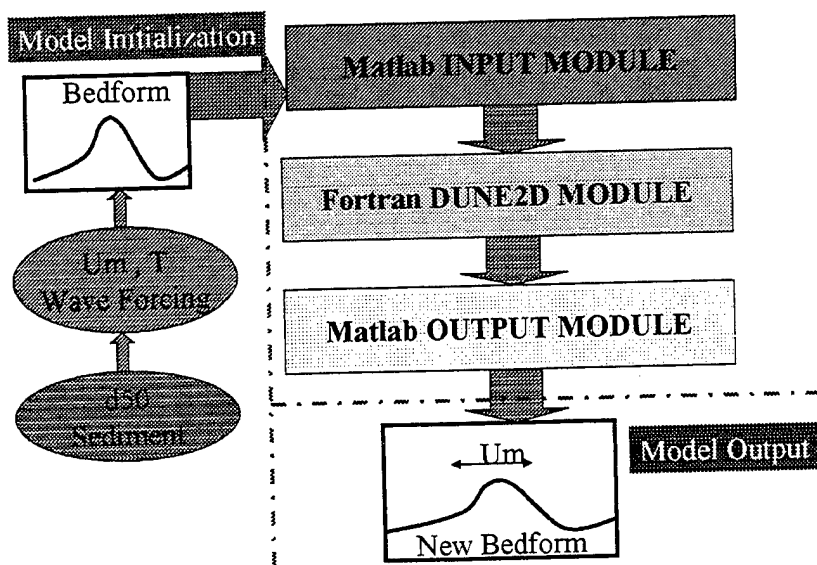


Figure C.1. General input/output flow diagram of modeling simulation.

### A. GENERAL I/O PROCEDURES

The first step to a morphology simulation focuses on determining the wave and current forcing dynamics. A Matlab program gathers user defined input concerning the ocean dynamics and sediment mean grain diameter. An \*.inp file is created. Second, a bedform \*.grd file is generated from field or experimental bedform data. A schematic diagram of the MATLAB programs used to generate the input file data is shown in Figure (C.2).

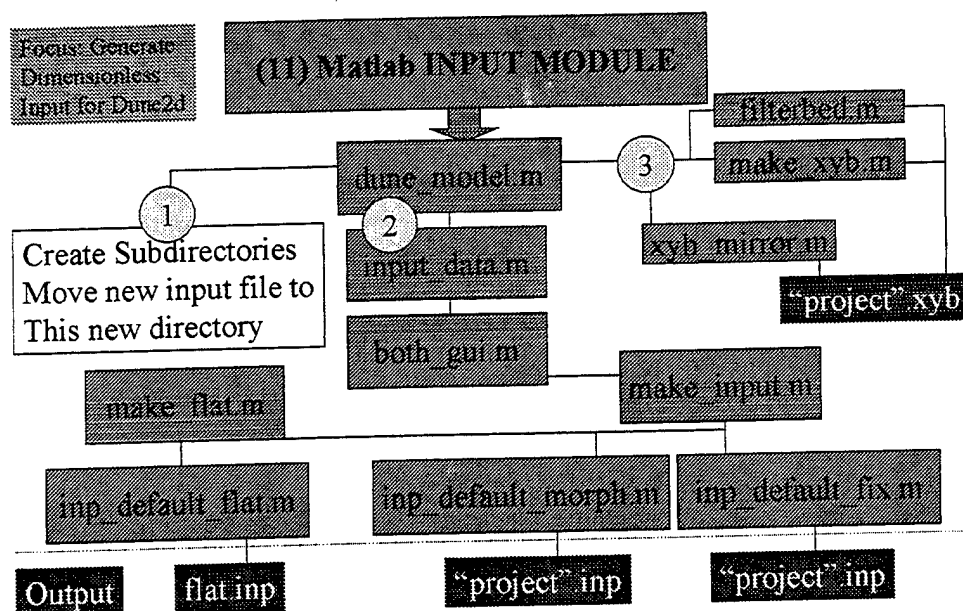


Figure C.2. DUNE2D input data flow of MATLAB programs.

Once all the input files are created. The first step of the morphology simulation is to run a hot file simulation run. The main purpose of the hot file run is to generate an initial solution to the flow field over a flat bed. The output generated by DUNE2D includes a \*.hot file at the end of each wave period of simulation. Normally, the hot file is generated over four complete wave periods. The \*.hot output file is used by the actual morphology simulation to help initiate the model flow solutions. If the hot file is not included, the morphology run from a "cold" start will typically not have convergence of the flow solution.

During the model simulation, output in ASCII format of specific single wave period averaged parameters (Table A.7) are placed into \*.meanbed files in the Unix simulation folder. MATLAB programs were developed to produce graphical data output. A summary of the programs and output options are included in Figure (C.2).

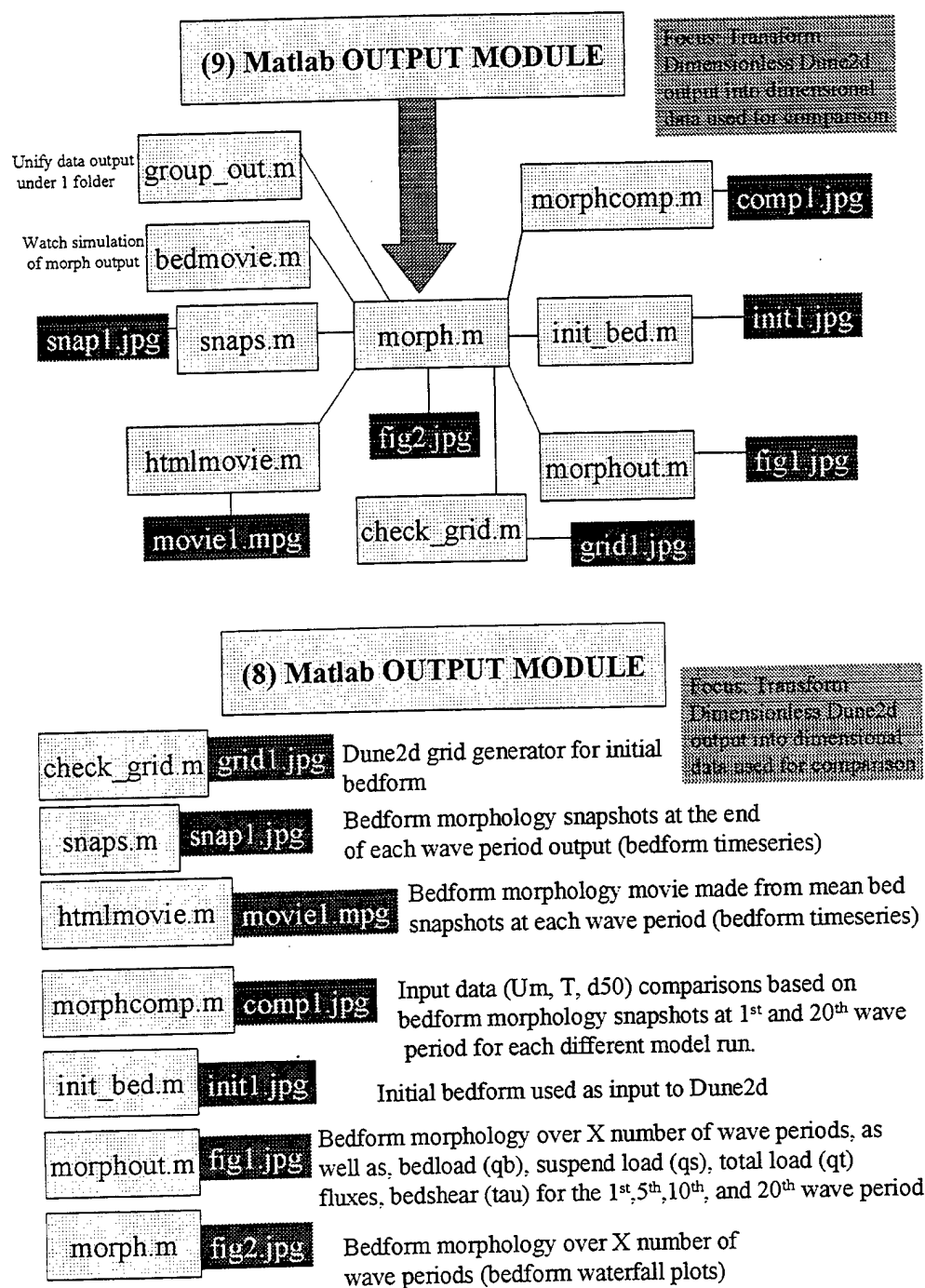


Figure C.2. DUNE2D output data flow of MATLAB programs.

## B. FIELD DATA TRANSFORMATION

More detail on the specific MATLAB programs used to transform field data into DUNE2D input variables and files are provided in Figure (C.3).

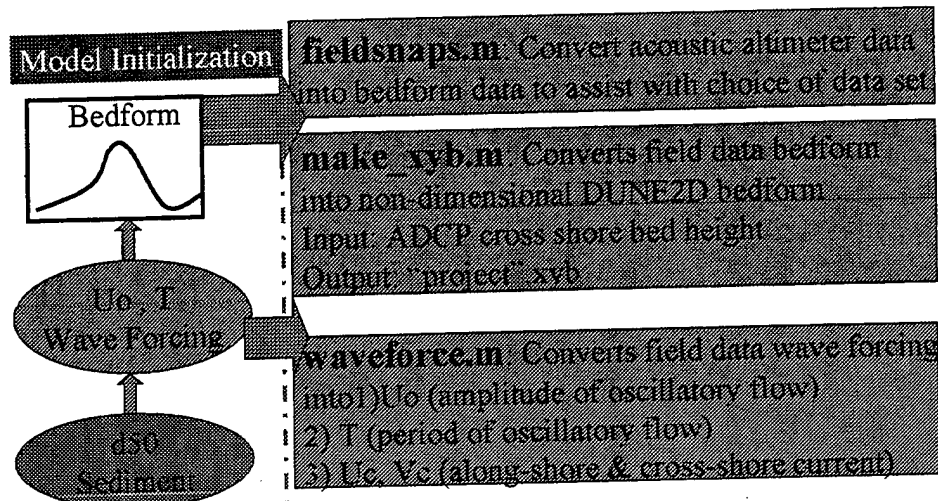


Figure C.3. MATLAB programs used to transform field data into model input.

### 1. Bedform Transformation

MATLAB program *make\_xyb.m* produces non-dimensional bedform (Figure C.4a-f.) in the form of an ASCII file \*.xyb, as seen in Appendix (B). Initially the field bedform data points (Figure C.4a.) are re-oriented so that the left end point starts at 0 meters, in both height and horizontal distance (Figure C.4b.). The boundary conditions require the bedform to be periodic on each end. This requires fictitious points to be added to the right end of the shifted bedform. The bedform was extended an additional 30% of the original bed to produce a gentler slope up towards the zero height line. Twenty additional points were used to linearly interpolate from the last original data point on the right side up to the height of the point on the left boundary (Figure C.4c). To ensure smooth ends for the fully periodic boundaries, a 10% cosine filter is applied to the

extended bedform (Figure C.4d). The filter, when applied, maintains most of the original roughness of the bedform except at the ends, where the smoothing takes place (Figure C.4e). The final step is to make the length and height of the bed non-dimensional by dividing through by a length scale,  $D$  (Figure C.4f). Further information on calculation of  $D$  can be found in Appendix (A).

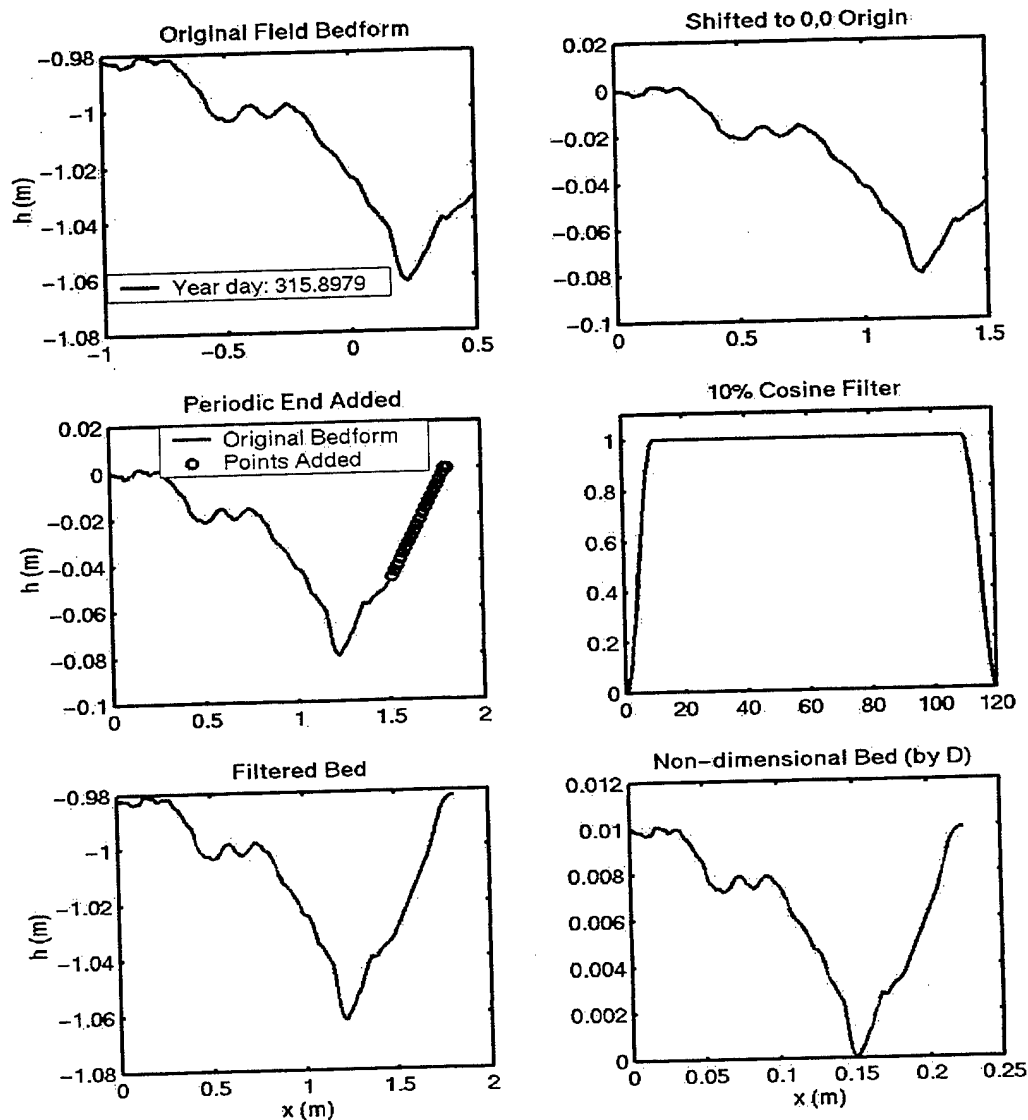


Figure C.4. Transformation of cross-shore field bedform data to DUNE2D non-dimensional bedform data.

## 2. Monochromatic Wave Dynamic Forcing Transformation

MATLAB program *waveforce.m* is used to determine the monochromatic sinusoidal wave forcing described by the oscillatory velocity amplitude and peak wave period that are incorporated into the input file, \*.inp. From the field measured  $u$  (along-shore) and  $v$  (cross-shore) velocity profiles of the BCDV profiler, the power spectrum can be found to determine the peak period,  $T$ , of the wave forcing. The oscillatory wave velocity amplitude is calculated as the equivalent sinusoidal velocity amplitude that gives the same wave variance as measured,

$$U_o = \sqrt{2} \sqrt{\sigma_u^2 + \sigma_v^2} \quad (C.1)$$

where  $\sigma_u^2$  and  $\sigma_v^2$  are the along-shore and cross-shore velocity component variances. This calculation is performed to get the best directional representation of the wave forcing over the bed.

Finally, mean values of the  $u$  and  $v$  velocity time series represent the along-shore and cross-shore currents, respectively.

## LIST OF REFERENCES

- Andersen, K.H., The Dynamics of Ripples Beneath Surface Waves and Topics in Shell Models of Turbulence, PH.D. dissertation, University of Copenhagen, 1999.
- Ardhuin, F., T. H. C. Herbers and W. C. O'Reilly, A Hybrid Eulerian-Lagrangian Model for Spectral Wave Evolution with Application to Bottom Friction on the Continental Shelf, *Journal of Geophysical Research*, In Press, 2001.
- Deigaard, R., J.B. Jakobsen, and J. Fredsoe, Net Sediment Transport Under Wave Groups and Bound Long Waves, *Journal of Geophysical Research*, 104 (C6), 13559-13575, 1999.
- Engelund, F., and J. Fredsoe, Sediment Ripples and Dunes, *Annu. Rev. Fluid Mech.*, 14, 13-37, 1982.
- Fredsoe, J., K. Andersen, and B. Mutlu Sumer, Wave Plus Current Over a Ripple-covered Bed, *Coastal Engineering*, 38, 177-221, 1999.
- Fredsoe, J., and R. Deigaard, *Mechanics of Coastal Sediment Transport*, World Scientific, River Edge, N.J. 1992.
- Nielsen, P., *Coastal Bottom Boundary Layers and Sediment Transport*, World Scientific, River Edge, N.J. 1992.
- Nielsen, P., Dynamics and Geometry of Wave-Generated Ripples, *Journal of Geophysical Research*, 86 (C7), 6467-6472, 1981.
- Open University Course Team, *Waves, Tides, and Shallow-water Processes*, Pergamon Press, N.Y., 1989.
- Soulsby, R., *Dynamics of Marine Sands*, Thomas Telford Publications, New York, N.Y., 1997.
- Soulsby, R.L., L. Hamm, G. Klopman, D. Myrhaug, R. R. Simmons and G. P. Thomas, Wave-current Interaction Within and Outside the Bottom Boundary Layer, *Coastal Engineering*, 21, 41-69, 1993.
- Stanton, T.P., Probing Ocean Wave Boundary Layers with a Hybrid Bistatic/Monostatic Coherent Acoustic Doppler Profiler, *Proceedings of the Microstructure Sensors in the Ocean Workshop*, Mt hood, 1996.

Stanton, T.P., High Resolution Acoustic Doppler Profiling of Velocity, Reynolds Stresses and Sediment Concentration in Wave Forced Boundary Layers, submitted to *Journal of Atmospheric and Oceanic Technology*, 2000.

Traykovski, P., A.E. Hay, J.D. Irish, and J.F. Lynch, Geometry, Migration, and Evolution of Wave Orbital Ripples at LEO-15, *Journal of Geophysical Research*, 104 (C1), 1505-1524, 1999.



## INITIAL DISTRIBUTION LIST

	No. of Copies
1. Defense Technical Information Center ..... 8725 John J. Kingman Road, Suite 0944 Ft. Belvoir, VA 22060-6218	2
2. Dudley Knox Library ..... Naval Postgraduate School 411 Dyer Road Monterey, CA 93943-5101	2
3. Oceanography Department, Code OC/Gd..... Naval Postgraduate School 833 Dyer Road, Rm. 328 Monterey, CA 93943-5122	1
4. Prof E.B. Thornton..... Oceanography Department, Code OC/Tm Naval Postgraduate School 833 Dyer Road, Rm. 328 Monterey, CA 93943-5122	2
5. Prof T.P. Stanton..... Oceanography Department, Code OC/St Naval Postgraduate School 833 Dyer Road, Rm. 328 Monterey, CA 93943-5122	2
6. Stephen Martin..... 8809 Newell Court Springfield, VA 22153	4
7. Harold P. Martin ..... 47 Amy Circle Bumpass, VA 23024	2